CORA Cork Open Research Archive
Cartlann Taighde Oscailte Chorcaí

Title	Power capture performance of hybrid wave farms combining different wave energy conversion technologies: The H-factor
Authors	Zheng, Siming;Zhang, Yongliang;Iglesias, Gregorio
Publication date	2020-05-24
Original Citation	Zheng, S., Zhang, Y. and Iglesias, G. (2020) 'Power capture performance of hybrid wave farms combining different wave energy conversion technologies: The H-factor', Energy, 204, 117920 (18pp). https://doi.org/10.1016/j.energy.2020.117920
Type of publication	Article (peer-reviewed)
Link to publisher's version	10.1016/j.energy.2020.117920
Rights	© 2020, Elsevier Ltd. All rights reserved. This manuscript version is made available under the CC BY-NC-ND 4.0 license. - https://creativecommons.org/licenses/by-nc-nd/4.0/
Download date	2026-11-04 09:40:12
Item downloaded from	https://hdl.handle.net/10468/10029



UCC
University College Cork, Ireland
Coláiste na hOllscoile Corcaigh

Title:

Power capture performance of hybrid wave farms combining different wave energy conversion technologies: the *H-factor*

Author names and affiliations:
Siming Zheng[a,b], Yongliang Zhang[b], Gregorio Iglesias[a,c]

[a] School of Engineering, Computing and Mathematics, University of Plymouth, Drake Circus, Plymouth PL4 8AA, UK
[b] State Key Laboratory of Hydroscience and Engineering, Tsinghua University, Beijing 100084, China
[c] MaREI Centre, Environmental Research Institute & School of Engineering, University College Cork, Ireland

Email address of each author:
Siming Zheng: siming.zheng@plymouth.ac.uk
Yongliang Zhang: yongliangzhang@tsinghua.edu.cn
Gregorio Iglesias: gregorio.iglesias@ucc.ie

Corresponding author:
Gregorio Iglesias
E-mail address: gregorio.iglesias@ucc.ie

Power capture performance of hybrid wave farms combining different wave energy conversion technologies: the *H-factor*

Abstract

In this paper we consider hybrid wave farms, in which different types of WEC are combined, through a case study involving oscillating water columns (OWCs) and point-absorbers (PAs). A new parameter, called "*H-factor*", is introduced to compare hybrid (multi-type) and conventional (single-type) wave farms in terms of wave power capture. We develop an *ad hoc* semi-analytical model to calculate the *H-factor* in a computationally efficient manner, and apply it to investigate how the *H-factor* and, consequently, the power capture, depend on: (i) the spacing and layout of the WECs, (ii) the type of WEC technology, and (iii) the wave conditions. We discuss the influence of these factors and, in the process, show that the *H-factor* is a valuable decision-aid tool. For specified wave conditions and layout limitations, a conventional wave farm may not be the most efficient option as a result of a destructive array effect, whereas a hybrid farm can be more efficient if a constructive hybrid effect occurs (if the *H-factor* value is above unity). This constructive hybrid effect can even overcome the destructive array effect for specified cases, demonstrating the potential advantage of hybrid wave farms relative to conventional wave farms.

Keywords: Oscillating water column; Point-absorber; Capture width factor; Wave energy; Wave power; Wave farm.

Nomenclature

A	incident wave amplitude
$\dot{A}_{i,j}$	motion/pressure response vector velocity of the i-th WEC oscillating in j-th mode
a_{PA}	array factor of a PA wave farm
c_{a}	the sound velocity in air
$\mathbf{C}_{\mathrm{d}}$	matrix of wave damping coefficients
$c_{\mathrm{h},n}$	PTO damping coefficient of PA n
$c_{\mathrm{p},n}$	PTO damping coefficient of OWC n
$\mathbf{C}_{\mathrm{PTO}}$	matrix of damping coefficients of PTO system in a wave farm
d_n	submerged depth of WEC n
$\mathbf{E}$	constraint matrix
$\boldsymbol{F}_{\mathrm{c}}$	restraining forces/moments to fix the OWC chambers
$\boldsymbol{F}_{\mathrm{e}}$	wave excitation volume/force acting on the wave farm
g	acceleration of gravity
H	hybrid effect factor
i	imaginary unit
$\mathbf{K}_{\mathrm{m}}$	mooring line restoring stiffness matrix
$k_{\mathrm{m},n}$	mooring line restoring stiffness of WEC n
$\mathbf{K}_{\mathrm{p}}$	a skew-symmetric matrix connecting the motions of OWC and its chamber
$\mathbf{K}_{\mathrm{s}}$	hydrostatic stiffness matrix of a wave farm
L	The distance between two OWCs/PAs in the same row/column

$\mathbf{M}$	mass matrix of a wave farm
M	number of OWCs in a wave farm
m_0	mass of PA
$\mathbf{M}_a$	matrix of added-mass coefficients
$\mathbf{M}_{PTO}$	matrix of mass coefficients of PTO system in a wave farm
N	number of PAs in a wave farm
p_i	air pressure inside the chamber of OWC i
P_{in}	incoming wave power per unit width of the wave front
p_{OWC}	power absorbed by an OWC in isolation
P_{OWC}	power absorbed by an OWC wave farm
p_{PA}	power absorbed by a PA in isolation
P_{PA}	power absorbed by a PA wave farm
q_{OWC}	array factor of an OWC wave farm
$R_{i,n}$	inner radius of OWC n
R_n	outer radius of WEC n
v_g	wave group velocity
V_n	air chamber volume of OWC n
$\dot{\boldsymbol{X}}$	motion/pressure response vector
η	wave power capture factor of a hybrid wave farm
η_{OWC}	wave power capture factor of an OWC in isolation
η_{PA}	wave power capture factor of a PA in isolation
ρ	density of sea water
ρ_0	density of static air
ω	angular wave frequency
$a_{(n)}^{(n)}$	added-mass of OWC n in isolation due to its air pressure oscillation
$a_{n,3}^{(n)}$	added-mass of OWC n in isolation due to its heave motion
$a_{(n)}^{n,3}$	heave added-mass of OWC n in isolation due to its air pressure oscillation
$a_{n,3}^{n,3}$	heave added-mass of WEC n in isolation due to its heave motion
$c_{(n)}^{(n)}$	radiation damping of OWC n in isolation due to its air pressure oscillation
$c_{n,3}^{(n)}$	radiation damping of OWC n in isolation due to its heave motion
$c_{(n)}^{n,3}$	heave radiation damping of OWC n in isolation due to its air pressure oscillation
$c_{n,3}^{n,3}$	heave radiation damping of WEC n in isolation due to its heave motion
OWC	Oscillating Water Column
PA	Point Absorber
PTO	Power Take-Off

WEC	Wave Energy Converter

1. Introduction

For wave energy to contribute significantly to decarbonizing the energy mix and meeting the carbon reduction targets, wave energy converters (WECs) will have to be deployed in arrays, or *wave farms*. Power extraction by wave farms has been the focus of intensive research (Babarit, 2010, 2013; Borgarino et al., 2012; Nader, 2013; Sarkar et al., 2014; Astariz and Iglesias, 2016a, 2016b; Veigas et al., 2015; Veigas and Iglesias, 2014; Konispoliatis and Mavrakos, 2016; Penalba et al., 2017). The variability of the resource at the site (Carballo et al. 2015a, 2015b), the power output of the WECs (Carballo and Iglesias, 2012; Malara and Arena, 2013; Lopez et al., 2016; Carballo et al., 2019) and, on this basis, the power output of the wave farm as a whole were investigated. Another relevant line of research concerns the optimization of WECs and WEC arrays (Veigas et al., 2014), often tackled by means of CFD (Lopez et al., 2014; Elhanafi et al., 2018; Guo et al., 2018). Finally, in the assessment of any wave energy project, the Levelised Cost of Energy plays a fundamental role. The economic viability of wave farms has also been investigated, e.g., Astariz and Iglesias (2015, 2016c) and Contestabile et al. (2016).

The benefits that can be obtained by combining wave and offshore wind energy systems have been investigated by, e.g., Astariz and Iglesias (2016d, 2016e) and Perez-Collazo et al. (2018a, 2018b), and a method was suggested to assess the feasibility of co-locating wave and offshore wind energy systems, based on the Co-location Feasibility Index (Astariz and Iglesias, 2017). These benefits range from a smoothed power output (Astariz and Iglesias, 2016f) to economies in O&M tasks (Astariz et al., 2018).

Research on wave farms has focused on arrays with one single wave energy conversion technology, i.e., one type of WEC. The possibility of combining different types of WECs in the same wave farm, forming a *hybrid* wave farm, has not been sufficiently investigated so far. Recently, a wave farm with two types of WECs was investigated from the point of view of wave-structure interaction (Zheng et al., 2018), without assessing the all-important energy production performance – one of the fundamental elements in assessing the economic viability of a wave project. This is the motivation for the present work, in which a hybrid farm consisting of two oscillating water columns (OWCs) and two point-absorbers (PAs) is considered and compared with non-hybrid or conventional wave farms (with only one type of technology).

The WECs in a wave farm are, by definition, in proximity; therefore, the wave interaction between individual WECs may be expected to play a role in the response and power performance of the system (e.g., Zhong and Yeung, 2019; Zheng et al., 2019a). Consequently, the total power captured by a wave farm consisting of N_0 WECs will in general be different from N_0 times the power of a single WEC working in isolation. This is known as the array or park effect, which can be assessed through the q-factor. Also known as *gain factor*, it is defined as the ratio of the maximum time-averaged power absorbed by the interacting WECs to the maximum time-averaged power absorbed by the WECs in isolation (McIver et al., 1995; Mavrakos and Kalofonos, 1997; Wolgamot, et al., 2012). Thus, the q-factor quantifies the influence of the hydrodynamic interactions within a given WEC array. Following Evans (1980) and Falnes (1980), the time-averaged power absorbed by a wave farm is the difference between

the excitation power and the radiated power. Therefore, the maximum time-averaged power absorbed by the farm can be evaluated from the wave excitation forces and the radiation damping matrix directly, without detailed consideration of the power take-off system (PTO). Mavrakos and Kalofonos (1997) employed this approach to compute the maximum power extraction of a wave farm and revealed that the *q*-factor was sensitive to variations in the configuration of the farm. This method was also used by Fitzgerald and Thomas (2007), who proved that for arrays of heaving hemispheres, the interaction of the *q*-factor over the entire range of incident wave directions, $[0, 2\pi]$, was equal to 2π. Later, Wolgamot et al. (2012) found that the directional behavior of the *q*-factor was valid under more general conditions, i.e., regardless of body dimensions and motion modes. However, in the above studies the wave farms were assumed to be composed of fully controlled WECs with both phase and amplitude optimized for the full range of wave conditions; in practice, however, such optimal control is not realistic.

In the case of an array of two semi-submerged cylinders moving only in the heave mode, Babarit (2010) calculated the *q*-factor by setting the PTO stiffness to zero, and tuning the PTO damping in order to achieve the maximum energy absorption at the natural frequency of an isolated device. Additionally, a modified factor denoted as q_{mod} was proposed as the ratio of the difference between the time-averaged power absorbed by a WEC in the farm and the time-averaged power absorbed by the same WEC in isolation, to the maximum time-averaged power absorbed by the WEC in isolation. q_{mod} was also adopted by Borgarino et al. (2012) and Renzi et al. (2014) to study the power absorption of a wave farm consisting of nine to twenty-five cylinder WECs and two to three flap-type WECs in the nearshore. Given that the value of q_{mod} is specific to each WEC in the wave farm, in the case of farms composed by many WECs many values of q_{mod} will need to be calculated, thus increasing the complexity of the performance evaluation.

Penalba et al. (2017) investigated the influence of the slenderness and the number of WECs in a wave farm on the hydrodynamic performance in realistic wave climates with a numerical method. The PTO damping coefficient was assumed to be the same for all the WECs in the farm, as no significant improvement had been reported from individually optimizing the PTO coefficients of each WEC (Ricci et al., 2007). The PTO damping coefficient was optimized for each sea state, as in the case of a single device. It was found that for farms consisting of no more than ten WECs, there was an optimal inter-device distance for maximizing the power absorption of the farm.

Besides the *q*-factor, the wave power capture factor, also known as the capture-width ratio, is of interest here. It is defined as the ratio of the time-averaged power absorbed by the wave farm to the mean wave power flux across a "characteristic width" of wave front. For an array of submerged spherical WECs, Wu et al. (2016) chose the sum of their diameters as the characteristic width. The wave power capture factor was also used to investigate the performance of an array of OWCs (Nader, 2013; Konispoliatis and Mavrakos, 2016), with the characteristic width set as the sum of the inner diameters of the OWC chambers. Major improvements were obtained for an array of OWCs of some specified value, with the OWCs either restrained or free-floating (Konispoliatis and Mavrakos, 2016).

For a wave farm consisting of a single type of WEC with a single geometry, either the *q*-factor or the wave power capture factor may be used to evaluate the performance of the farm

and the array effect. However, neither factor serves to assess the effect of combining different types of WECs in a hybrid wave farm, relative to a conventional, single-type wave farm. This is the motivation to propose in this work a new parameter, the *H-factor*. We develop a semi-analytical model and apply it to a hybrid wave farm consisting of two types of WECs: Oscillating Water Columns (OWCs) and Point-Absorbers (PAs).

In addition to the power performance, the motion and pressure response of the WECs in the hybrid wave farm are considered. A number of case studies are considered, including free-floating or fixed OWCs, and different layouts. The PTO damping coefficients are optimized for each wave condition.

The rest of this paper is organized as follows. The motion response equations, the expressions of power absorption and the *H-factor* are given in Section 2. The comparison between the hybrid wave farm and conventional OWCs/PAs farm in terms of wave power extraction can be found in Section 3, along with the effects of incident wave direction and distance between adjacent OWCs/PAs. Finally, conclusions are drawn in Section 4.

2. Assessment of response and power generation

Although all OWCs and PAs in a hybrid wave farm (Fig. 1) may be free to oscillate independently in six degrees of freedom, it is hard in practice to make full use of all these motions in absorbing wave power.

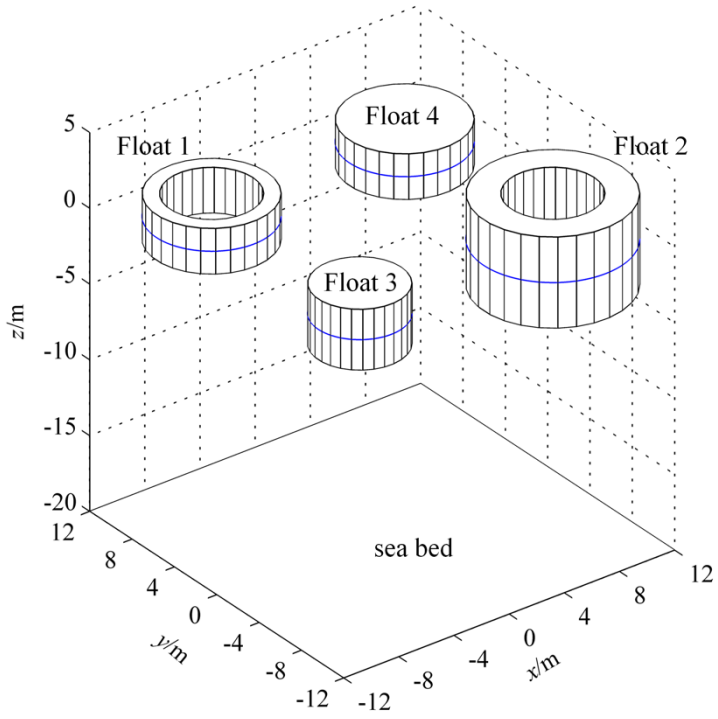


Fig. 1. Top view of a hybrid wave farm consisting of two OWCs and two PAs (adapted from Zheng et al. , 2018)

Since each PA is connected to a linear generator resting on the seabed, it is the heave motion that primarily provides the power. In the case of offshore OWCs, both floating and fixed types may be used in a hybrid wave farm. In this paper two cases of hybrid wave farm are considered (Fig. 2). In Case I the OWCs are attached to the seabed by mooring lines, and the

chambers can oscillate in all degrees of freedom on the water surface. In Case II the OWCs are fixed to the seabed by rigid piles. The response and power absorption in both cases are evaluated below.

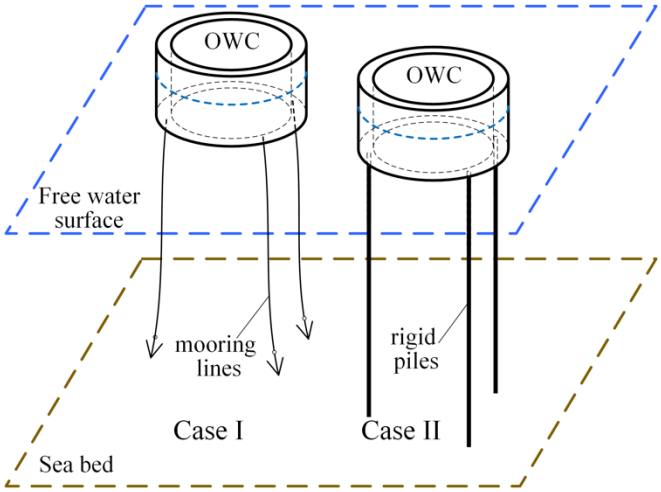


Fig. 2. Sketch of OWCs in the two cases of hybrid wave farm.

2.1 Motion and pressure response

The hybrid wave farm is exposed to regular monochromatic waves. The farm is composed of $M+N$ WECs in total, in which the first M WECs are OWCs and the remaining N WECs are PAs. The volume flux through the turbines in the OWCs is assumed to be proportional to the chamber air pressure following Zheng and Zhang (2018), Zheng et al. (2019a, 2019b) and He et al. (2019). For the hybrid wave farm with free floating OWCs under regular waves of small amplitude, the matrix equation of motion of the farm in the frequency domain can be written as:

$$\left[-\mathrm{i}\omega\left(\mathbf{M}_{\mathrm{a}}+\mathbf{M}_{\mathrm{PTO}}+\mathbf{M}\right)+\left(\mathbf{C}_{\mathrm{d}}+\mathbf{C}_{\mathrm{PTO}}\right)+\mathrm{i}\left(\mathbf{K}_{\mathrm{s}}+\mathbf{K}_{\mathrm{m}}\right)/\omega+\mathbf{K}_{\mathrm{p}}\right]\dot{\boldsymbol{X}}=\boldsymbol{F}_{\mathrm{e}}, \quad (1)$$

where $\dot{\boldsymbol{X}}$ is the motion/pressure response vector expressed as $\dot{\boldsymbol{X}}=\left[\dot{A}_{1,1},\cdots,\dot{A}_{1,6},\dot{A}_{2,1},\cdots,\dot{A}_{M+N,6},p_1,\cdots,p_M\right]^{\mathrm{T}}$, in which the motion response of the WECs are given in terms of velocities, $\dot{A}_{i,j}$ is the velocity of the i-th WEC oscillating in j-th mode (j=1~6 represents surge, sway, heave, roll, pitch and yaw, respectively), p_i is the air pressure inside the chamber of OWC i, 'T' denotes the transpose; $\boldsymbol{F}_{\mathbf{e}}$ represents the wave excitation volume/force acting on the wave farm, and it is a $(7M+6N)\times1$ vector, written as $\boldsymbol{F}_{\mathrm{e}}=\left[F_{\mathrm{e}}^{1,1},\cdots,F_{\mathrm{e}}^{1,6},F_{\mathrm{e}}^{2,1},\cdots,F_{\mathrm{e}}^{M+N,6},F_{\mathrm{e}}^{(1)},\cdots,F_{\mathrm{e}}^{(M)}\right]^{\mathrm{T}}$, in which $F_{\mathrm{e}}^{i,j}$ is the wave excitation forces/moments acting on the i-th WEC in j-th mode, $F_{\mathrm{e}}^{(i)}$ is the wave excitation volume flux of OWC i. ω is the angular wave frequency; i represents the imaginary unit; $\mathbf{M_a}$ and $\mathbf{C_d}$ are two $(7M+6N)\times(7M+6N)$ square matrices of added-mass and radiation damping coefficients due to wave radiation, which can be calculated, together with $\boldsymbol{F}_{\mathbf{e}}$, with the theoretical model proposed

in Zheng et al. (2018). $\mathbf{M_{PTO}}$ is a diagonal matrix of mass coefficients of Power Take-Off system (PTO) in the wave farm, the diagonal elements of which can be written as

$$diag\left(\mathbf{M}_{\mathrm{PTO}}\right)=1/\left(c_{\mathrm{a}}^{2}\rho_{0}\right)\left[\mathbf{0}_{1\times 6(M+N)},V_{1},V_{2},\cdots,V_{M}\right]^{\mathrm{T}}. \tag{2}$$

Here, the M non-vanishing elements in $\mathbf{M_{PTO}}$ are used to consider the effect of compressibility of air in the OWC chambers, in which c_{a} is the sound velocity in air, ρ_0 is the static air density, V_n is the air chamber volume. $\mathbf{C_{PTO}}$ represents a diagonal matrix of the damping coefficients of PTO in the wave farm written as

$$diag\left(\mathbf{C}_{\mathrm{PTO}}\right)=\left[\mathbf{0}_{1\times 6M},0,0,c_{\mathrm{h},1},0,0,0,0,0,c_{\mathrm{h},2},\cdots,c_{\mathrm{h},N},0,0,0,c_{\mathrm{p},1},c_{\mathrm{p},2},\cdots,c_{\mathrm{p},M}\right]^{\mathrm{T}},. \tag{3}$$

in which $c_{\mathrm{h},n}$ (n=1, 2,…, N) represent the PTO damping induced by the linear generator connected to PA n; $c_{\mathrm{p},n}$ (n=1, 2,…, M) represent the PTO damping coefficients induced by the turbine in the OWC n, which depend on the static air density, the rotational speed of turbine blades, the outer diameter of the turbine rotor, and the design, number and setup of turbines (Martins-rivas and Mei, 2009; Lovas et al., 2010; Zheng and Zhang, 2018). $\mathbf{M}$ and $\mathbf{K}_{\mathrm{s}}$ are the mass matrix and hydrostatic stiffness matrix of the hybrid wave farm. As the effect of hydrostatic stiffness on OWCs has already been included in the radiation coefficients (Falnes, 2002), different from those for traditional floats, no separate term is required in $\mathbf{K}_{\mathrm{s}}$ for OWCs. The diagonal elements of $\mathbf{M}$ and $\mathbf{K}_{\mathrm{s}}$ are

$$diag\left(\mathbf{M}\right)=\left[m_{1},m_{1},m_{1},I_{1},I_{1},I_{1}',\cdots,I_{M+N},I_{M+N}',\mathbf{0}_{1\times M}\right]^{\mathrm{T}}, \tag{4}$$

$$diag\left(\mathbf{K}_{\mathrm{s}}\right)=\rho g\left[0,0,s_{1},s_{1}',s_{1}',0,\cdots,s_{M+N}',0,\mathbf{0}_{1\times M}\right]^{\mathrm{T}}, \tag{5}$$

where, if we assume both OWCs and PAs are half submerged at equilibrium with the mass uniformly distributed all over their volume, the non-vanishing elements in $\mathbf{M}$ and $\mathbf{K}_{\mathrm{s}}$ can be expressed as:

$$m_{n}=\rho\pi\left(R_{n}^{2}-\xi_{n,M}R_{\mathrm{i},n}^{2}\right)d_{n}, \tag{6}$$

$$I_{n}=\frac{1}{12}\rho\pi d_{n}\left(R_{n}^{2}-\xi_{n,M}R_{\mathrm{i},n}^{2}\right)\left[3\left(R_{n}^{2}+\xi_{n,M}R_{\mathrm{i},n}^{2}\right)+4d_{n}^{2}\right], \tag{7}$$

$$I_{n}'=\frac{1}{2}\rho\pi d_{n}\left(R_{n}^{4}-\xi_{n,M}R_{\mathrm{i},n}^{4}\right), \tag{8}$$

$$s_{n}=\pi\left(R_{n}^{2}-\xi_{n,M}R_{\mathrm{i},n}^{2}\right), \tag{9}$$

$$s_{n}'=\frac{1}{4}\pi\left(R_{n}^{2}-\xi_{n,M}R_{\mathrm{i},n}^{2}\right)\left[\left(R_{n}^{2}+\xi_{n,M}R_{\mathrm{i},n}^{2}\right)-2d_{n}^{2}\right], \tag{10}$$

in which d_n and R_n denote the submerged depth and the outer radius of WEC n, respectively; $R_{\mathrm{i},n}$ is the inner radius of OWC n; $\xi_{n,M}$=1 for $n\leq M$, whereas $\xi_{n,M}$ vanishes for $n>M$; ρ is the density of sea water.

$\mathbf{K}_{\mathrm{m}}$ is the restoring stiffness matrix induced by the mooring lines. The mooring system is not the focus of this work; therefore, the effect of the mooring lines is assumed to be negligible,

i.e., $\mathbf{K}_{\mathrm{m}}=\mathbf{0}$. $\mathbf{K}_{\mathrm{p}}$ is a skew-symmetric matrix used to consider the force on the horizontal chamber's wall of the OWC due to its inner pressure and the volume flux created by the heaving motion of the OWC chamber. There are 2M non-vanishing elements in the matrix in total. For the upper triangular part of $\mathbf{K}_{\mathrm{p}}$, the non-vanishing element at the 6(n-1)+3-th row and the 6(M+N)+n–th column (n=1,2,…, M) is $-\pi R_{\mathrm{i},n}^2$. For the lower triangular part, the element at the 6(M+N)+n–th row and the 6(n-1)+3-th column (n=1,2,…, M) is $\pi R_{\mathrm{i},n}^2$.

For the hybrid wave farm of Case II, all OWC chambers are strictly restrained, thus a 6M×1 scale vector, denoted as $\boldsymbol{F}_{\mathrm{c}}$, representing the restraining forces/moments to fix the chambers, should be introduced into the new matrix equation:

$$\begin{bmatrix} \left[-\mathrm{i}\omega\left(\mathbf{M}_{\mathrm{a}}+\mathbf{M}_{\mathrm{PTO}}+\mathbf{M}\right)+\left(\mathbf{C}_{\mathrm{d}}+\mathbf{C}_{\mathrm{PTO}}\right)+\mathrm{i}\mathbf{K}_{\mathrm{s}}/\omega+\mathbf{K}_{\mathrm{p}}\right] & \mathbf{E}_{(7M+N)\times 6M} \\ \mathbf{E}^{\mathrm{T}}_{(7M+N)\times 6M} & \mathbf{0}_{6M\times 6M} \end{bmatrix} \begin{Bmatrix} \dot{\boldsymbol{X}} \\ \boldsymbol{F}_{\mathrm{c}} \end{Bmatrix} = \begin{Bmatrix} \boldsymbol{F}_{\mathrm{e}} \\ \mathbf{0}_{6M\times 1} \end{Bmatrix}, \tag{11}$$

where $\mathbf{E}$ is a (7M+N)×6M constraint matrix consisting of a 6M×6M identity matrix and a (M+N)×6M zero matrix below the identity matrix. The rest matrices are all the same as defined above for Cases I.

The motion/pressure response of the hybrid wave farm of Cases I and II can be obtained by solving the matrix equations Eqs. (1) and (11).

2.2 Power absorption

In regular waves, the time-averaged absorbed power of the hybrid farm for Cases I and II can be expressed in the same equation as:

$$P=\frac{1}{2}\left(\sum_{n=1}^{M} c_{\mathrm{p},n}\left|p_n\right|^2+\sum_{n=M+1}^{M+N} c_{\mathrm{h},n}\left|\dot{A}_{n,3}\right|^2\right)=\frac{1}{2}\left(\mathbf{H}\dot{\boldsymbol{X}}\right)^{\dagger}\mathbf{C}_{\mathrm{PTO}}\mathbf{H}\dot{\boldsymbol{X}}, \tag{12}$$

where $\mathbf{H}$ is a diagonal matrix written as

$$diag\left(\mathbf{H}\right)=\left[\mathbf{0}_{1\times 6M},0,0,1,0,0,0,0,0,1,\cdots,1,0,0,0,\mathbf{1}_{1\times M}\right]^{\mathrm{T}}, \tag{13}$$

and '†' denotes the complex-conjugate transpose.

The wave capture factor, also called the capture width ratio, can be defined by

$$\eta=\frac{P}{2P_{\mathrm{in}}\left(\sum_{n=1}^{M}R_{\mathrm{i},n}+\sum_{n=M+1}^{M+N}R_n\right)}=\frac{1}{4P_{\mathrm{in}}}\frac{\sum_{n=1}^{M}c_{\mathrm{p},n}\left|p_n\right|^2+\sum_{n=M+1}^{M+N}c_{\mathrm{h},n}\left|\dot{A}_{n,3}\right|^2}{\sum_{n=1}^{M}R_{\mathrm{i},n}+\sum_{n=M+1}^{M+N}R_n}, \tag{14}$$

where P_{in} represents the incoming wave power per unit width of the wave front given by:

$$P_{\mathrm{in}}=\frac{\rho g A^2 v_{\mathrm{g}}}{2}, \tag{15}$$

in which v_{g} denotes wave group velocity.

2.3 *H-factor*

For a wave farm consisting of one type of WECs with the same geometry, the "*q*-factor", defined as the ratio of the wave power absorbed by the wave farm to N_0 (the number of WECs in the farm) times that produced by a WEC in isolation, has been widely used by researchers to evaluate the constructive or destructive effect induced by the hydrodynamic interaction among the WEC array (Borgarino et al., 2012; Penalba et al., 2017). Similar to the "*q*-factor" for conventional wave farms, it would be possible to define a "q^*-factor" to address the hydrodynamic interaction within the hybrid WEC array. This "q^*-factor" would be expressed as

$$q^* = \frac{P}{Mp_{\mathrm{OWC}} + Np_{\mathrm{PA}}} = \frac{\left(MR_{\mathrm{OWC}} + NR_{\mathrm{PA}}\right)\eta}{MR_{\mathrm{OWC}}\eta_{\mathrm{OWC}} + NR_{\mathrm{PA}}\eta_{\mathrm{PA}}}, \tag{16}$$

where p_{OWC} and p_{PA} are the power absorbed by each OWC and PA in isolation, respectively. η_{OWC} and η_{PA} are the capture factors of the OWC and PA in isolation, respectively. However, this q^*-factor would not be able to distinguish the effect induced by combining different types of WECs in a hybrid wave farm from the "array effect" of conventional wave farms (the two effects would be included in the q^*-factor).

In this work, to better understand the effect caused by the *hybrid* character of a wave farm, a new factor called "*H-factor*" is introduced as follows:

$$H = \frac{P}{P_{\mathrm{OWC}}\dfrac{M}{M+N} + P_{\mathrm{PA}}\dfrac{N}{M+N}} = \frac{P}{Mq_{\mathrm{OWC}}p_{\mathrm{OWC}} + Nq_{\mathrm{PA}}p_{\mathrm{PA}}}. \tag{17}$$

where P_{OWC} and P_{PA} are the power absorbed by the wave farm when the WECs are all OWCs and all PAs, respectively. q_{OWC} and q_{PA} are the corresponding so-called "*q*-factors" of the array of conventional OWCs and PAs, respectively.

Unlike the *q*-factor, which quantifies the hydrodynamic interaction between the WECs in a wave farm (i.e., the *array effect*), the *H-factor* quantifies the effect of combining different types of WECs in a hybrid wave farm (i.e., the *hybrid effect*). For $H>1$ and $H<1$, the *hybrid* farm performs better or worse than the equivalent conventional (single type of device) wave farm, i.e., the *hybrid effect* is constructive or destructive, respectively – or in other words, positive or negative. In the case of a conventional wave farm, i.e., one that consists of a single type of device (whether OWC or PA), $H\equiv 1$, and the *hybrid effect* is neutral or non-existent.

Eq. (17) can also be written as follows, after expressing P, p_{OWC} and p_{PA} by means of the capture factors η, η_{OWC} and η_{PA}:

$$H = \frac{\left(MR_{\mathrm{OWC}} + NR_{\mathrm{PA}}\right)\eta}{MR_{\mathrm{OWC}}\eta_{\mathrm{P1}} + NR_{\mathrm{PA}}\eta_{\mathrm{P2}}} = \frac{\left(MR_{\mathrm{OWC}} + NR_{\mathrm{PA}}\right)\eta}{MR_{\mathrm{OWC}}q_{\mathrm{OWC}}\eta_{\mathrm{OWC}} + NR_{\mathrm{PA}}q_{\mathrm{PA}}\eta_{\mathrm{PA}}}, \tag{18}$$

in which R_{OWC} and R_{PA} represent the inner radius and radius of each OWC and PA, respectively; η_{P1} and η_{P2} represent the capture factors of the farm consisting of conventional OWCs and PAs, respectively, satisfying $\eta_{\mathrm{P1}}=q_{\mathrm{OWC}}\eta_{\mathrm{OWC}}$ and $\eta_{\mathrm{P2}}=q_{\mathrm{PA}}\eta_{\mathrm{PA}}$.

3. Results and discussion

The model presented in this paper may be used to solve the problem of a hybrid wave farm consisting of multiple OWCs and PAs with different scales and physical parameters. In this section we consider a case study in which all the OWCs have the same outer radius R_n, inner radius $R_{\mathrm{i},n}$, draught d_n, and PTO damping coefficient $c_{\mathrm{p},n}$, and all the PAs have the same radius

R_n, draught d_n, and PTO damping coefficient $c_{\mathrm{h},n}$. Both $c_{\mathrm{p},n}$ and $c_{\mathrm{h},n}$ are considered variable and dependent of wave frequency.

The geometries of OWCs and PAs selected are those previously adopted by Nader (2013), Konispoliatis and Mavrakos (2016) and Göteman (2017), respectively, with the following parameters: h=20 m; PA: R_n/h=0.14, d_n/h=0.024; OWC: R_n/h=0.25, $R_{\mathrm{i},n}/h$=0.2, d_n/h=0.2.

The PTO damping coefficients $c_{\mathrm{h},n}$ and $c_{\mathrm{p},n}$ are selected based on the following principles. For all PAs in both Cases I and II, the value of $c_{\mathrm{h},n}$ is selected as the optimum coefficient of the same PA freely floating and working in isolation. As a symmetrical cylinder floating in isolation, the heave motion of PA is decoupled from the other degrees of freedom, thus

$$c_{\mathrm{h},n}=\sqrt{\left(c_{n,3}^{n,3}\right)^2+\left[\omega\left(m_n+a_{n,3}^{n,3}\right)-\left(\rho g s_n+k_{\mathrm{m},n}\right)/\omega\right]^2}\,. \tag{19a}$$

For all OWCs in Case I, $c_{\mathrm{p},n}$ is selected as the optimum coefficient of the same OWC when freely floating in isolation. As the OWC is a symmetrical cylinder with a moonpool, both the pressure inside the OWC chamber and the chamber motion in heave mode are decoupled from the chamber motion in the other degrees of freedom. From the standpoint of power absorption, the OWC in Case I in isolation is similar to a motion system consisting of the air pressure and the OWC chamber oscillating in the heave mode only. Given that only the air pressure oscilation is used to capture wave power, the optimal $c_{\mathrm{p},n}$ may be written as

$$c_{\mathrm{p},n}=\sqrt{\kappa_1^2+\kappa_2^2}\,, \tag{19b}$$

where κ_1 and κ_2 are two real parameters introduced from

$$\kappa_1+\mathrm{i}\kappa_2=c_{(n)}^{(n)}-\mathrm{i}\omega\left[a_{(n)}^{(n)}+V_n/\left(c_a^2\rho_0\right)\right]-\frac{\left(c_{(n)}^{n,3}-\pi R_{\mathrm{i},n}^2-\mathrm{i}\omega a_{(n)}^{n,3}\right)\left(c_{n,3}^{(n)}+\pi R_{\mathrm{i},n}^2-\mathrm{i}\omega a_{n,3}^{(n)}\right)}{c_{n,3}^{n,3}-\mathrm{i}\omega\left(a_{n,3}^{n,3}+m_n\right)+\mathrm{i}\left(\rho g s_n+k_{\mathrm{m},n}\right)/\omega}\,. \tag{19c}$$

For all OWCs in Case II, $c_{\mathrm{p},n}$ are considered equal to the optimum coefficient of the same OWC when being strictly restrained in isolation condition. This is a motion system with only one degree of freedom, i.e., oscillation of the pressure inside the OWC chamber, thus the optimum coefficient can be easily obtained as:

$$c_{\mathrm{p},n}=\sqrt{\left(c_{(n)}^{(n)}\right)^2+\omega^2\left[a_{(n)}^{(n)}+V_n/\left(c_{\mathrm{a}}^2\rho_0\right)\right]^2}\,. \tag{19d}$$

The dimensionless PTO damping coefficients can be defined as follows:

$$\overline{c}_{\mathrm{h},n}=\frac{c_{\mathrm{h},n}}{\omega\rho R_n^3};\ \ \overline{c}_{\mathrm{p},n}=\frac{\omega\rho c_{\mathrm{p},n}}{R_{\mathrm{i},n}}. \tag{20}$$

In Fig. 3, the maximum power capture factor of an isolated floating/fixed OWC and an isolated PA, together with the corresponding nondimensional optimal PTO damping coefficients calculated from Eqs. (19) and (20), are plotted against kh. For kh ranging from 0.1 to 6.0, η_{OWC}-kh presents a bimodal and a unimodal curves for Case I and Case II, respectively. The first peak value of η_{OWC} for Case I is 0.25 at kh=3.1, only 32.5 percentages as large as that of the single peak for Case II, which is 0.78 occurring at kh=3.2. The second peak value of η_{OWC} for Case I is 0.52, occurring at kh=4.4. The peaks at kh=3.1 and 4.4, might be explained by the resonances induced by water column oscillation and the heave motion of OWC chamber, respectively. Note that for kh<2.5, there is nearly no power can be extracted by the free floating

OWC (Case I), so is it for *kh*>5.5. Due to no power radiated away induced by oscillation of the chamber, the fixed OWC (Case II) shows an overall better power absorption ability for all the tested wave conditions, except at 4.2<*kh*<4.6, where the second peak of η_{OWC} for Case I happens. For the isolated PA, as *kh* increases from 0.1 to 6.0, η_{PA} increases first, and then stabilizes at 0.4 after *kh* reaching 4.0. Compared with the fixed OWC, PA performances better in capturing power for short waves. Whereas the fixed OWC is prefered for 2.2<*kh*<3.6, where for some specified wave conditions, the maximum power capture factor of OWC can be two times as large as that of PA. Variation of $\overline{C}_{\mathrm{p},n}$ and $\overline{C}_{\mathrm{h},n}$ with *kh* shows rather different trends (Fig. 3b). $\overline{C}_{\mathrm{h},n}$ decreases monotonically with the increasing of *kh*. While, $\overline{C}_{\mathrm{p},n}$ -*kh* turns to be a unimodal curves curve, regardless of Case I and Case II, whereas the the peaks of $\overline{C}_{\mathrm{p},n}$ for Case I and Case II occur at different *kh*, i.e. 4.4 and 3.2, which correspond to the resonant frequencies of water column oscillation and OWC chamber heaving motion, respectively. In addition, the peak value of $\overline{C}_{\mathrm{p},n}$ for Case I is much larger than that for Case II. In the following parts, the optimal PTO damping coefficients for isolated OWC and PA (Fig. 3b) are adopted in the wave farm of OWCs and/or PAs.

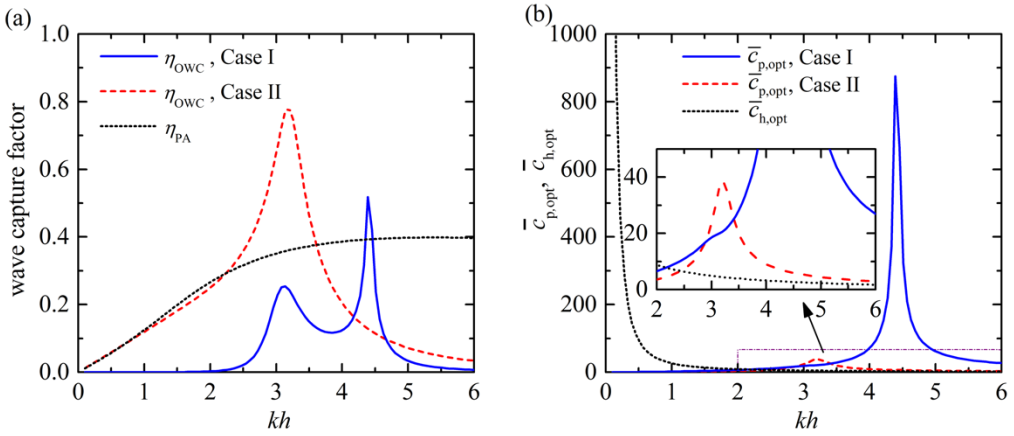


Fig. 3. Wave power capture factor of a floating/fixed OWC and a PA in isolation, and optimized PTO damping versus *kh*.

Two array configurations of a hybrid wave farm consisting of two OWCs and two PAs, denoted as #H1 and #H2, respectively, are examined in this section (Fig. 4). The OWCs and PAs are placed at the tops of a square. The distance between two OWCs/PAs in the same row/column is *L*.

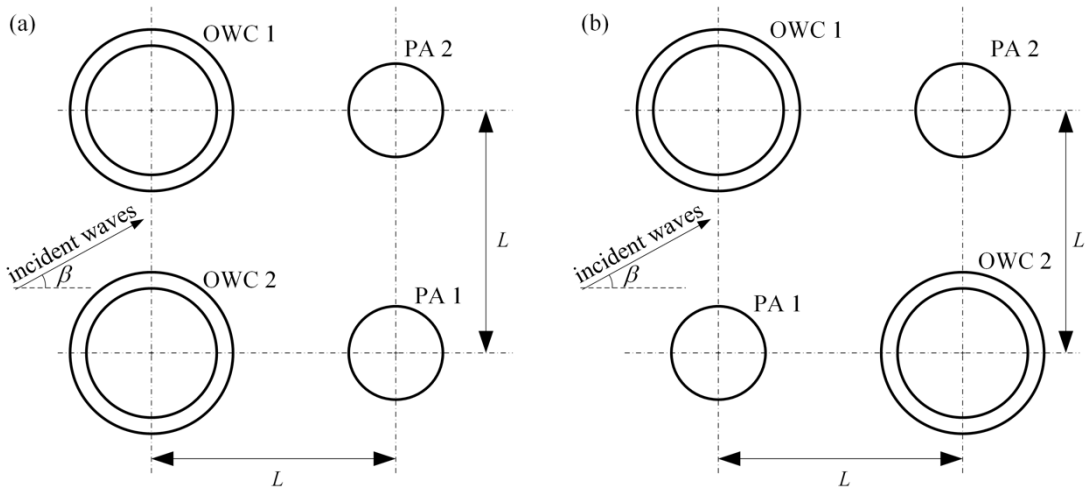


Fig. 4. Schematic of a hybrid wave farm consisting of two OWCs and two PAs, (a) # H1; (b) # H2 (Zheng et al., 2018)

3.1 Comparison between hybrid and conventional OWCs/PAs farm

To make a comparison between hybrid wave farms and conventional OWCs/PAs farms, apart from the hybrid wave farm configurations (Fig. 4), two conventional OWCs/PAs farms are also considered (Fig. 5), denoted as # P1 and # P2, respectively. The OWCs/PAs have all the same geometries and PTO damping coefficients (Figs. 3b and 4).

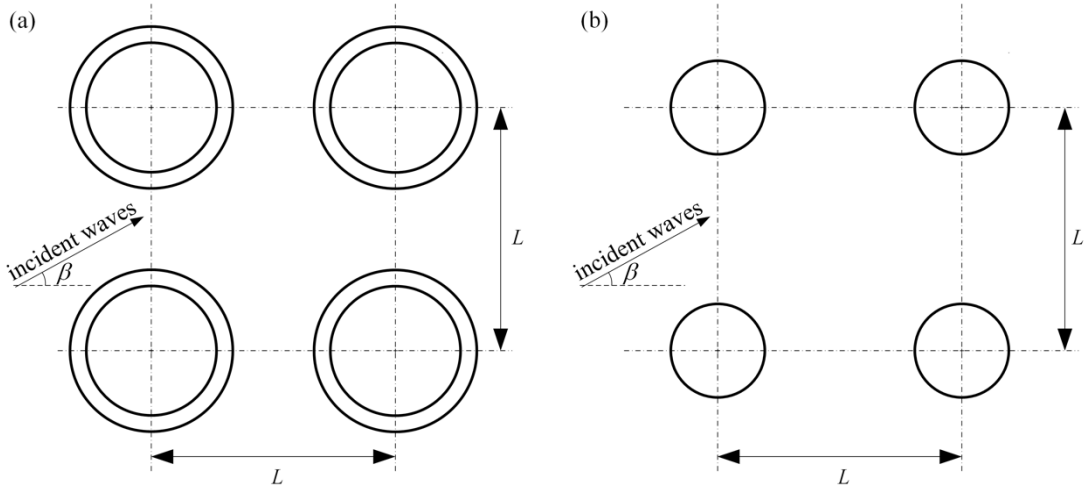


Fig. 5. Schematic of a conventional wave farm consisting of a single type of device: (a) OWCs, # P1; (b) PAs, # P2.

Figure 6 presents a power capture factor comparison between the hybrid wave farm # H1, # H2, the conventional wave farm # P1 (all OWCs) and # P2 (all PAs), and the isolated OWC and PA for both Cases I and II, L/h=0.75, β=0. The hydrodynamic interaction between the PAs of # P2 plays a constructive role for 4.6<kh<6.0, where the maximum power capture factor of # P2 is 0.45, going up by 12.5% compared with that of the isolated PA. Whereas for the rest wave conditions, especially for 3.0<kh<4.5, a destructive effect of the interaction in # P2 is found. Compared with isolated free floating OWC, constructive effect for # P1 of Case I appears at 3.6<kh<4.0 and 4.6<kh<6.0. Note that a rather destructive influence also occurs at

3.0<*kh*<3.5. For the hybrid wave farm ＃H1 of Case I, its power capture factor (η_{H1}) for *kh*<2.5 is approximately 50% of that of ＃P2 (η_{P2}). This is mainly due to the much less power absorption by the free floating OWCs for these wave frequencies. When comparing with ＃P1 of Case I, ＃H1 of Case I holds an obviously larger power capture factor for almost all the studied wave conditions. If OWCs and PAs are arranged at diagonal corners of the square, i.e., ＃H2 (see Fig. 4b), rather than in parallel with wave front line (＃H1, see Fig. 4a), power absorption of the hybrid farm can be significantly improved for *kh* ranging from 2.8 to 5.5, except around *kh*=4.4 (strictly, 4.3<*kh*<4.5) where the sharp peak occurs.

Comparison of Figs. 6a and 6b shows that power extraction of the farm consisting of fixed OWCs (Case II) is much larger than that of the farm with OWCs free floating. This is clearly a consequence of the performance difference between the isolated OWC of Cases I and II as discussed above about the results illustrated in Fig. 3a. The power capture factors of these six farms/single WEC for Case II are quite close to each other for any specified wave frequency in the range of *kh*<2.0 (Fig. 6b). Although the "wave capture factor-*kh*" curves representing isolated fixed OWC and the array of fixed OWCs (＃P1 of Case II) are both unimodal, the latter one holds a lower peak, nevertheless a wider bandwidth. Specifically, for 2.5<*kh*<3.9, $\eta_{P1}<\eta_{OWC}$, and the peak value of η_{P1} is 0.55 at *kh*=3.1, much smaller than that of η_{OWC}, which is 0.78 occurring at *kh*=3.2. Whereas for 1.3<*kh*<2.5 and 3.9<*kh*<5.8, $\eta_{P1}>\eta_{OWC}$. For the two deployments of hybrid wave farm both consisting of two fixed OWCs and two PAs (＃H1 and ＃H2 of Case II), ＃H1 holds a better performance in power absorption at 2.4<*kh*<4.1, where for ＃H1 and ＃H2 of Case I the comparing result is mostly opposite as discussed above. For short waves, the hybrid wave farm ＃H2 absorbs more power from ocean waves than ＃H1. It is worth noting that, for 3.3<*kh*<3.7, η_{H1} is obviously larger than both η_{P1} and η_{P2}. This implies that, for a certain range of wave conditions, mixing OWCs and PAs in the wave farm are rather beneficial to the power absorption of wave farm.

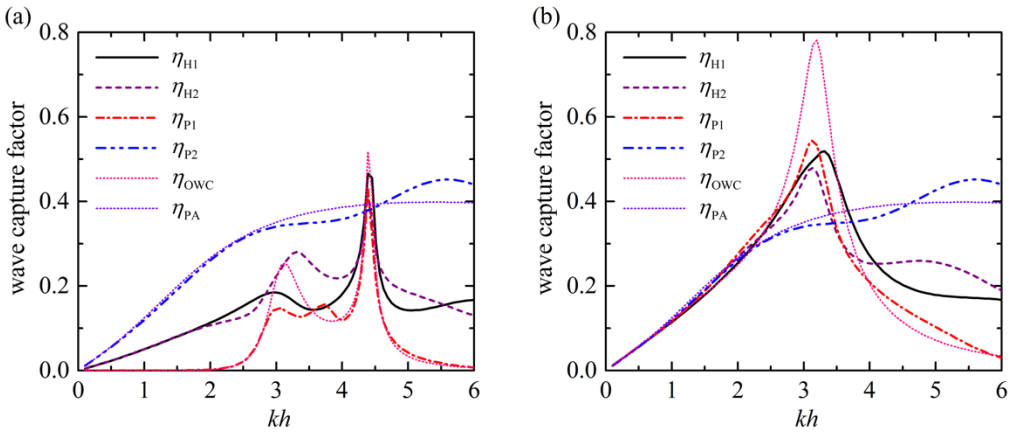


Fig. 6. Wave power capture factor of different configurations of hybrid/conventional wave farms versus *kh* for *L*/*h*=0.75, β=0: (a) Case I; (b) Case II.

Power absorption capacity of the wave farm (Fig. 6) is given in terms of wave capture factor, which does not separate the effect induced by mixing different type of WECs in the wave farm, i.e., hybrid effect, from the effect of hydrodynamic interaction among WECs array, i.e., array effect.

To have a better understanding of the effect caused by the *hybrid* WECs in the hybrid wave farm, power capture ability of ＃H1 and ＃H2 for Case I and II, L/h=0.75, β=0 in terms of the new proposed factor, i.e., "*H-factor*", are plotted in Fig. 7. For kh<2.0 of Case I (Fig. 7a), both H_{H1} and H_{H2} equal to 1.0 approximately, implying a negligible hybrid impact for these wave conditions. This also applies for ＃H2 of Case II for kh <3.0 as shown in Fig. 7b. As kh increases towards 6.0, the values of H_{H1} and H_{H2} for Case I and II oscillate around 1.0, which means that, for L/h=0.75, β=0, constructive and destructive hybrid effect appear alternately with the variation of wave conditions. In Case I (Fig. 7a), for 2.0<kh<2.7, H_{H1}>1 and H_{H2}<1; while for 3.0<kh<3.6, H_{H1}<1 and H_{H2}>1. That is to say, hybrid effect plays opposite roles for different deployment of the hybrid wave farm consisting of free floating OWCs (Case I) for those wave conditions. Such opposite hybrid effect can also be found for the hybrid wave farm with fixed OWCs (Case II, Fig. 7b), for wave conditions: 3.3<kh<4.0 and 4.3<kh<5.7. Note for 3.3<kh<3.6, opposite hybrid effect happens not only for different deployments of hybrid wave farm, it also occurs for the same deployment by using different cases of OWCs. Take ＃H1 as an example: if free floating OWCs are adopted in such hybrid wave farm (Case I), we have H_{H1}<1 for 2.7<kh<4.0, however for the same range of wave conditions, if all the OWCs are fixed (Case II), on the contrary, H_{H1}>1 is obtained. The smallest value of H_{H1} for Case I is only 0.62 at kh=3.7; While for Case II, H_{H1} peaks at kh=3.5, reaching 1.35.

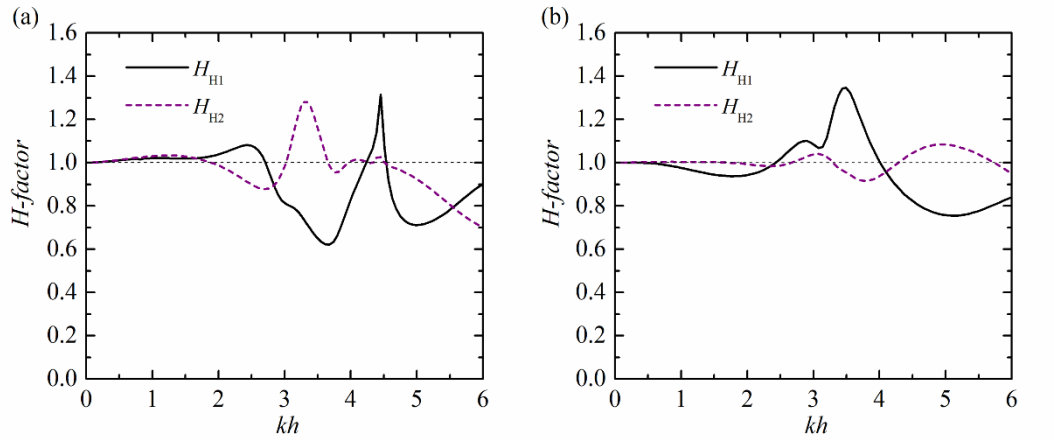


Fig. 7. *H-factor* of different configurations of hybrid wave farms versus kh for L/h=0.75, β=0: (a) Case I; (b) Case II.

The exact values of the *H-factor* together with the corresponding q^*-factor, q-factor (q_{OWC} and q_{PA}) for some selected wave numbers are presented in Table 1. For kh=3.5, although the q-factor values for conventional OWCs (Case II) and PAs wave farms are only 0.721 and 0.936, respectively, demonstrating the destructive array-effect, the q^*-factor of the hybrid wave farm ＃H1 (Case II) reaches 1.074. This proves that this hybrid wave farm greatly benefits from the dramatic constructive hybrid-effect (H_{H1}=1.345). In the case of kh=6.0, although the q^*-factor of the hybrid wave farm ＃H1 (Case I) is q^*_{H1}=0.997, which looks acceptable, the corresponding *H-factor* is only 0.901, indicating a destructive hybrid-effect and revealing the weakness of the hybrid wave farm ＃H1. It is apparent in these examples that the *H-factor* is useful in revealing the advantage or disadvantage, as the case may be, of the hybrid wave farm

relative to a conventional wave farm, and that this information cannot be obtained from the q^*-factor.

Table 1. *H-factor* of a hybrid wave farm (two different array configurations, i.e., #H1 and #H2) with L/h=0.75, β=0 and the corresponding q^*-factor, q-factor (q_{OWC} and q_{PA}) for different wave numbers (kh).

	q-factor q_{OWC}		q-factor q_{PA}	q^*-factor q^*_{H1}		q^*-factor q^*_{H2}		*H-factor* H_{H1}		*H-factor* H_{H2}	
kh	Case I	Case II		Case I	Case II	Case I	Case II	Case I	Case II	Case I	Case II
0.5	1.036	0.966	0.982	0.993	0.971	0.994	0.975	1.011	0.998	1.013	1.003
1.0	1.030	0.969	0.960	0.980	0.942	0.989	0.969	1.021	0.976	1.030	1.004
1.5	1.015	1.040	0.961	0.980	0.950	0.989	1.008	1.019	0.945	1.029	1.003
2.0	0.984	1.104	0.980	1.018	0.991	0.967	1.044	1.038	0.943	0.987	0.993
2.5	1.015	1.018	0.989	1.069	1.025	0.891	0.993	1.079	1.018	0.899	0.987
3.0	0.679	0.774	0.970	0.677	0.898	0.819	0.859	0.813	1.085	0.982	1.037
3.5	0.895	**0.721**	**0.936**	0.599	**1.074**	1.070	0.761	0.650	**1.345**	1.162	0.954
4.0	0.961	1.019	0.928	0.779	0.972	0.945	0.908	0.831	1.005	1.008	0.939
4.5	0.870	1.291	0.982	1.023	0.882	0.928	1.121	1.103	0.823	1.001	1.045
5.0	1.254	1.433	1.074	0.778	0.869	1.010	1.243	0.712	0.757	0.924	1.084
5.5	1.330	1.278	1.133	0.893	0.896	0.919	1.197	0.782	0.777	0.805	1.037
6.0	**1.040**	0.897	**1.108**	**0.997**	0.912	0.776	1.032	**0.901**	0.841	0.702	0.951

3.2 Effect of incident wave direction

In this section, the effect of the incident wave direction (β) on the power absorption of the hybrid wave farm is investigated. First, the frequency response of wave capture factor of the farm with conventional OWCs/PAs (#P1 and #P2) under regular waves propagating in different directions (β=0, π/8 and π/4) is evaluated (Fig. 8). The effect induced by increasing β from 0 to π/4 can be generally divided into three levels: negligible for long waves, enhanced effect for medium waves and inhibited effect for short waves (Table 2).

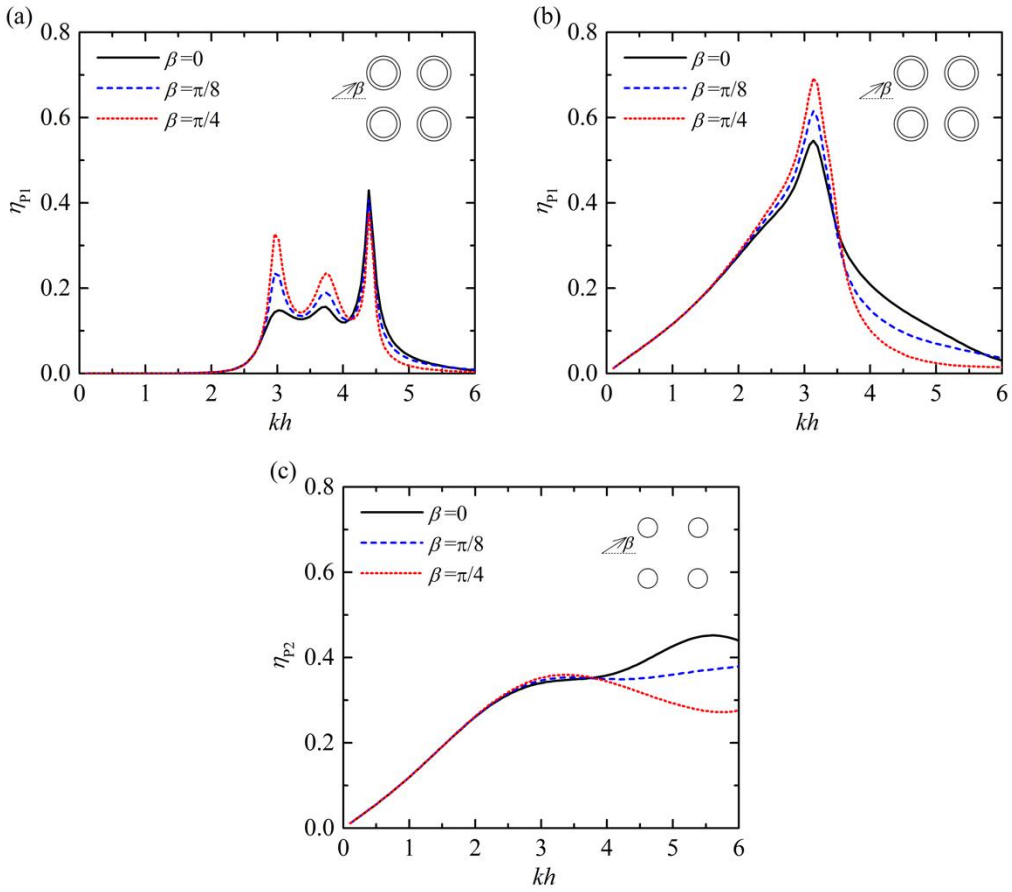


Fig. 8. Power capture factor of conventional wave farms versus kh for different β, L/h=0.75: (a) OWCs farm (Case I); (b) OWCs farm (Case II); (c) PAs farm.

Table 2. Frequency ranges and levels of effect of β.

Wave farm	negligible effect	enhanced effect	inhibited effect
#P1 (Case I)	kh<2.8	2.8<kh<4.1	4.2<kh<5.6
#P1 (Case II)	kh<2.2	2.2<kh<3.4	3.6<kh<5.7
#P2	kh<2.5	2.5<kh<3.7	3.9<kh<6.0

For the wave farm of PAs (i.e., #P2), the inhibited effect strength of β at 3.9<kh<6.0 is much stronger than in the case of the enhanced effect, occurring at 2.5<kh<3.7. Due to the symmetries of the deployment of #P1 and #P2, the power absorbed by the conventional wave farm with β=0 is the same as with β=π/2 and π. Similarly, β=π/8 and π/4 may also be used to represent situations with β=-π/8 and -π/4, respectively.

Figure 9 illustrates the variation in power capture factor of the hybrid wave farm #H1 (η_{H1} for Cases I and II) with kh for different β ranging from 0 to π with step π/4. The main effect of β for Case I occurs at kh>2.5 (Fig. 9a). For 2.9<kh<4.0, η_{H1} stays at a rather low level for incident waves coming from the OWCs side, i.e., β=0 and β=π/4, generally below 0.17. By contrast, when waves impinge from the side of the two PAs, i.e., β=3π/4 and π, the response of η_{H1} peaks at 0.43 and 0.47 for β=3π/4 and π, respectively, both appearing at kh=3.2. For 4.6<kh<6.0, the hybrid wave farm #H1 has an obviously better performance in extracting power from waves incoming at β=π/2 and π compared with β=0 and, especially, π/4 and 3π/4. This

rule also applies to #H1 with all OWCs fixed for 4.2<*kh*<6.0 (Case II, Fig. 9b). Such results do not appear as a surprise, for both arrays of conventional OWCs/PAs are better at absorbing power for short waves with a smaller β (Fig. 8). However, if we review the wave capture factor response of the conventional wave farms #P1 and #P2 (see Fig. 8) at 2.8<*kh*<3.5, where both η_{P1} (Cases I and II) and η_{P2} reach the smallest at β=0 (π/2 and π), and have a comparison with the response of η_{H1} (Cases I and II, see Fig. 9), a completely opposite effect of β on power absorption of the hybrid wave farms is observed, for η_{H1} achieves the largest at β=π (equivalent to β=0 for #P1 and #P2) in some certain subrange among 2.8<*kh*<3.5. This interesting phenomenon can be clearly explained using the *H-factor* (Fig. 10). Although both #P1 and #P2 capture the least power (i.e., worst array effect) at β=π, for 2.8<*kh*<3.4 and 3.2<*kh*<3.6 for Cases I and II, respectively (Fig. 8), the corresponding *H-factor*, H_{H1}, on the contrary, is the largest (i.e., best hybrid effect, Fig. 10), and the latter overcomes the former, leading to a better power absorption for β=π than β with any other values (Fig. 9). This implies that the hybrid effect, which can be quantified through the *H-factor* proposed in this work, may in fact overcome the destructive array effect. It should also be noted that the hybrid effect does not control the power absorption for all wave conditions. For example, H_{H1} for β=3π/4 is larger than that for β=0 in 4.5<*kh*<5.4 and 4.2<*kh*<4.9 for Cases I and II, respectively (Fig. 10), while due to the contrary β-based array effect happened in these wave conditions as demonstrated in Fig. 8, less power can be captured for β=3π/4 compared with β=0 (Fig. 9).

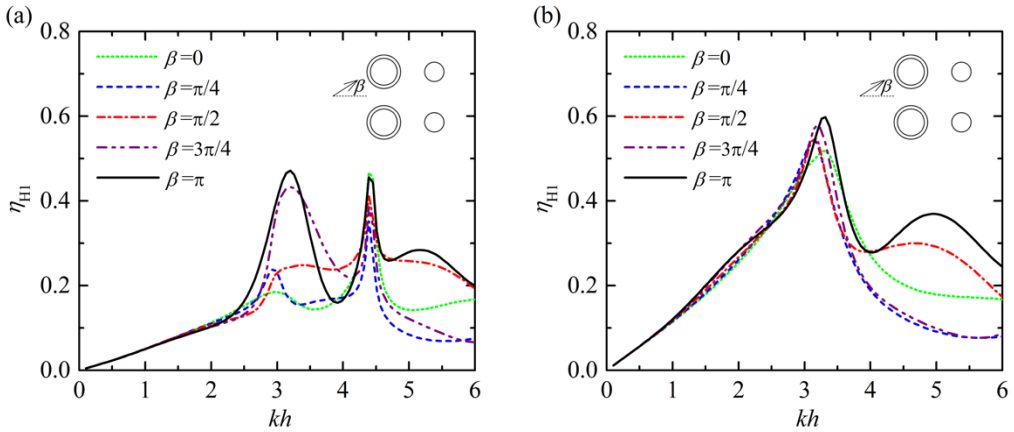


Fig. 9. Power capture factor of the hybrid wave farm #H1 versus *kh* for different β, *L*/*h*=0.75: (a) Case I; (b) Case II.

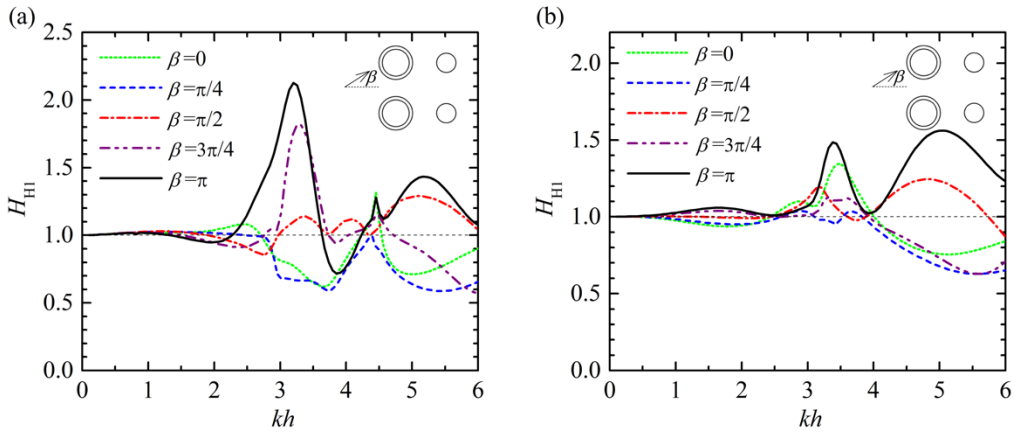


Fig. 10. *H-factor* of the hybrid wave farm # H1 versus *kh* for different β, *L*/*h*=0.75: (a) Case I; (b) Case II.

As discussed above, the better performance of the hybrid wave farm #H1 at $\beta=\pi$ with all OWCs free floating or fixed for $4.6<kh<6.0$ and $4.2<kh<6.0$, respectively, is likely due to a better array effect. From Fig. 10 we infer that $H_{H1}>1.0$ is satisfied for all these wave conditions, and can be even as large as 1.43 and 1.56, occurring at $kh=5.2$ and 5.0, respectively. This indicates that the better performance of the hybrid wave farm #H1 at $\beta=\pi$ results not only from the constructive array effect but also the constructive hybrid effect. This constructive hybrid effect of #H1 at $\beta=\pi$ for short waves can be explained from the point of wave reflection and transmission. The scale of PA in terms of radius and draft is smaller than that of the OWC, hence when the waves propagate from the PAs side, after being partially absorbed by the PAs, they can pass through the PAs toward the OWCs to be further absorbed by the OWC. Furthermore, thanks to the large wet area of the OWC, some waves are also reflected from the OWC towards the PAs, which are thus excited. However, if waves propagate from the OWCs side a significant part of wave power will be reflected by the OWCs, resulting in less power being transmitted to the PAs. For #H1, Case II, there is yet one more advantage: $H_{H1}>1.0$ applies to all wave conditions (Fig. 10b).

We now turn to the hybrid wave farm #H2, in which the two OWCs and two PAs are arranged at the two diagonal corners (Fig. 4b). The frequency response of η_{H2} and H_{H2} for the farm of Cases I and II under waves from different incident directions is presented in Figs. 11 and 12, respectively. For #H2 with all OWCs free floating (Case I), Figs. 11a and 12a, η_{H2} and H_{H2} depend strongly on β when *kh* ranges between 3.0 and 4.0. Unlike the performance of #H1 in $3.0<kh<4.0$, #H2 presents a better power absorption in terms of both η_{H2} and H_{H2} at $\beta=\pi/4$, rather than $\beta=\pi$ for #H1. η_{H2} and H_{H2} for $\beta=\pi/4$ reach their peak values 0.62 and 2.61, respectively, both at $kh=3.3$, where the corresponding values of η_{H2} and H_{H2} for $\beta=-\pi/4$ are only 0.20 and 0.83, less than one third of those for $\beta=\pi/4$, demonstrating the strong dependence on the incidence direction. Generally, for $3.0<kh<4.0$, the more β is away from $\pi/4$, the less H_{H2} and also the less power can be captured by #H2 (Case I).

The role of β is also significant in the case of #H2 with all OWCs fixed (Case II, Figs. 11b and 12b), and even for a wider range of *kh*. For $\beta=\pi/4$, $H_{H2}>1.0$ is satisfied for $1.5<kh<4.0$, and H_{H2} is also larger than those for any other value of β studied (Fig. 12b). After taking consideration of the influence of β on the array effect, i.e., not enhanced for all $1.5<kh<4.0$ but

even inhibited for large frequencies (see Fig. 8 and Table 2), the final power absorption of #H2 (Case II) for $\beta=\pi/4$ turns to have a larger value for only $1.5<kh<3.8$. Note for $kh>4.1$, on the contrary, H_{H2} for $\beta=\pi/4$ is the smallest one among different β (see Fig. 12b), which, with account of the inhibited influence of β on array effect for both #P1 (Case II) and #P2 as listed in Table 2, results in the worst power absorption (Fig. 11b).

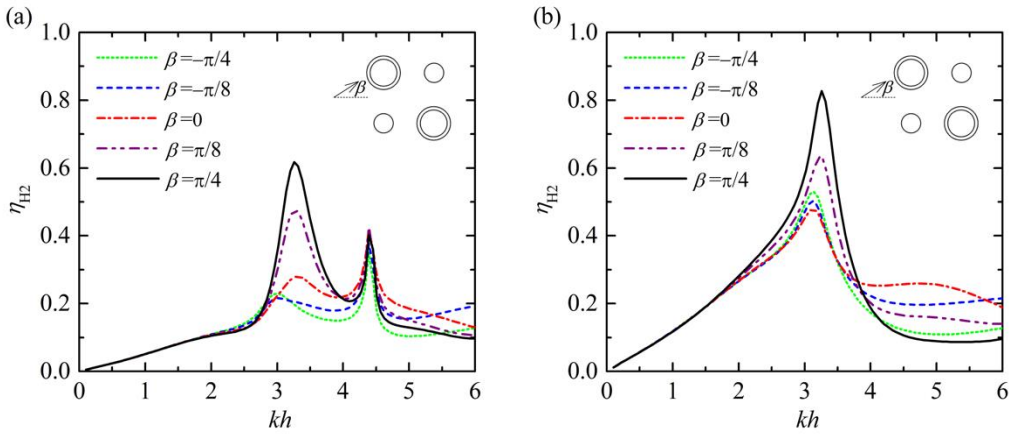


Fig. 11. Power capture factor of the hybrid wave farm #H2 versus kh for different β, $L/h=0.75$: (a) Case I; (b) Case II.

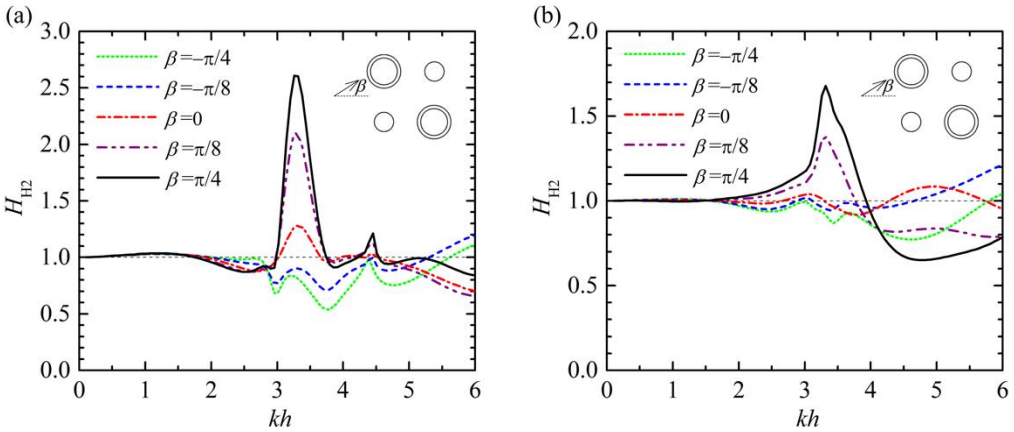


Fig. 12. *H-factor* of the hybrid wave farm #H2 versus kh for different β, $L/h=0.75$: (a) Case I; (b) Case II.

3.3 Effect of distance between two OWCs/PAs in the same row/column

We have learnt from Section 3.2 that, $\beta=\pi$ and $\pi/4$ are good choices for the hybrid wave farms #H1 and #H2, respectively, for some specified wave conditions and $L/h=0.75$. Hence, in this section, we discuss separately the effect of L/h on the performance of wave farms with $\beta=\pi$ and $\pi/4$ employed for #H1 and #H2. Before that, however, we consider the power capture factor of the conventional wave farm versus kh for different L/h is plotted in Fig. 13. Both the amplitude of the first peak of η_{P1} and η_{P2} and their corresponding kh are found to be affected by L/h. Detailed results are listed in Table 3.

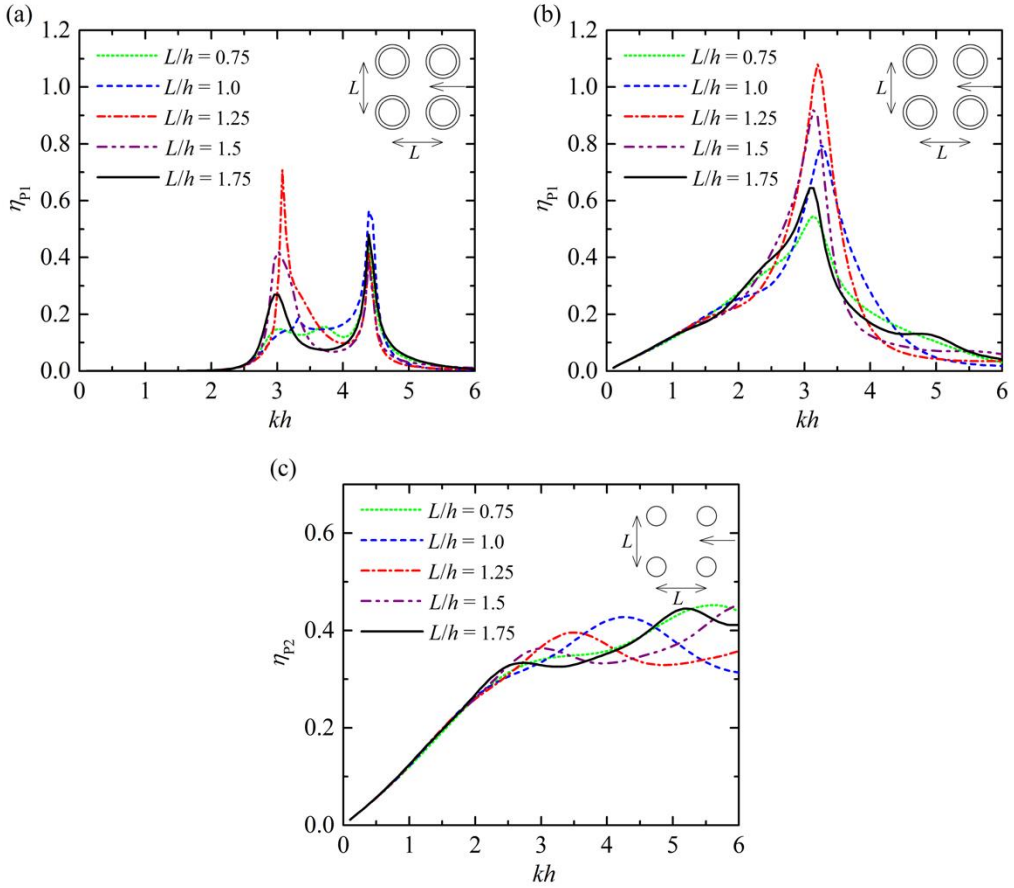


Fig. 13. Power capture factor of the conventional wave farm versus *kh* for different *L*/*h*, $\beta = \pi$: (a) OWCs farm of Case I; (b) OWCs farm of Case II; (c) PAs farm.

Table 3. First peak value of wave capture factor of #P1 (Cases I and II), #P2 and the corresponding *kh* for different *L*/*h*, $\beta=\pi$.

		L/*h*=0.75	*L*/*h*=1	*L*/*h*=1.25	*L*/*h*=1.5	*L*/*h*=1.75
#P1 (Case I)	first peak value of η_{P1}	0.15	0.18	0.71	0.42	0.27
	corresponding *kh*	3.02	3.32	3.08	3.02	2.96
#P1 (Case II)	first peak value of η_{P1}	0.55	0.80	1.08	0.92	0.64
	corresponding *kh*	3.14	3.26	3.20	3.14	3.14
#P2	first peak value of η_{P2}	0.45	0.43	0.40	0.36	0.33
	corresponding *kh*	5.58	4.27	3.50	3.02	2.72

For OWCs wave farm (#P1), as *L*/*h* increases from 0.75 to 1.75, the first peak value increases up to a maximum, then decreases. By contrast, for the PAs (#P2) studied, the first peak value decreases all the time with the increase of *L*/*h*. The wave farm (whether #P1 or #P2) with any specified *L*/*h* can absorb more power than the other farms with different *L*/*h* for a certain range of wave conditions (Fig. 13), but it may also capture the least for other wave conditions. A discussion on the effect of the spacing between WECs on the power absorption of a conventional (single type of device) wave farm consisting of OWCs/PAs can be found in

(Nader, 2013; Konispoliatis and Mavrakos, 2016; Andrés et al., 2014; Borgarino et al., 2012; Penalba et al., 2017).

Figures 14 and 15 present how power capture factor and *H-factor* of hybrid wave farm #H1 (Cases I and II) are affected by L/h. For the hybrid wave farm with all OWCs free floating (Fig. 14a), the maximum values of the first peak of η_{H1} for L/h=1.25 and 1.5 are achieved at kh=3.2 and 3.1, respectively. The first peak value of the farm with L/h =0.75 is a little smaller compared to L/h =1.25 and 1.5, and the corresponding conventional farms with L/h =0.75 are not attractive in extracting power either (Fig. 13), while thanks to the wider and stronger constructive hybrid effect occurring at 2.3<kh<3.6 and 4.3< kh <6.0 (Fig. 15a), #H1 with L/h =0.75 holds a wider bandwidth of peak at 2.5< kh <4.0 and a larger capture factor at 4.7< kh <5.6. It should also be noted that H_{H1} for L/h =1.0 is larger than 1.0 for nearly all the kh ranging from 0.1 to 6.0, and the power capture factor around kh =4.0 is much better than the farms with the other values of L/h. What is better, different from those with other L/h, #H1 with L/h =1.0 is almost never the worst one in capturing power for any wave conditions.

For #H1 of Case II, as shown in Fig. 14b, L/h =1.25 performs better than the others for wave conditions around kh =3.2 from the view of peak value of η_{H1} and its bandwidth. This is contributed to by both the array effect (Fig. 13) and the constructive hybrid effect (Fig. 15b). H_{H1}>1 applies to all wave conditions for L/h =1.0, especially at kh=3.3 and 5.0, where two peaks occur (Fig. 15b). Similarly, η_{H1}- kh for L/h =1.0 (Fig. 14b) also present a bimodal curve and it could be welcome for the sea site with bimodal type wave conditions.

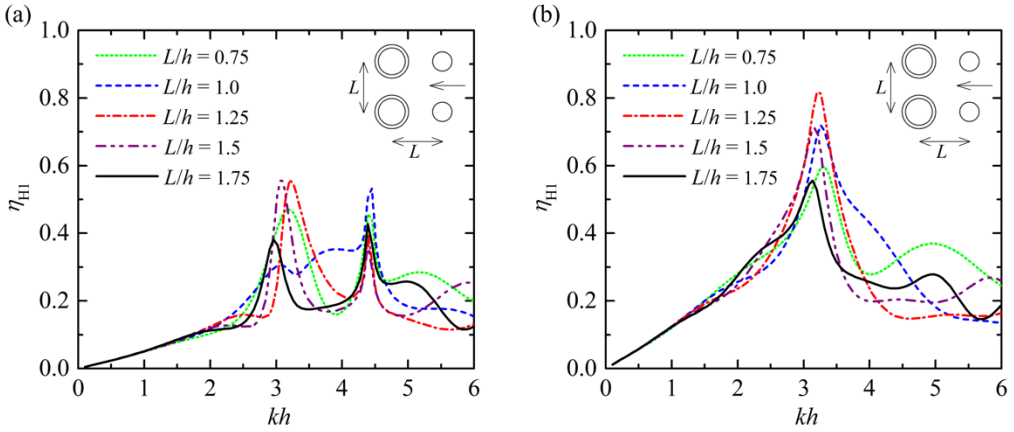


Fig. 14. Power capture factor of the hybrid wave farm #H1 versus kh for different L/h, β=π: (a) Case I; (b) Case II.

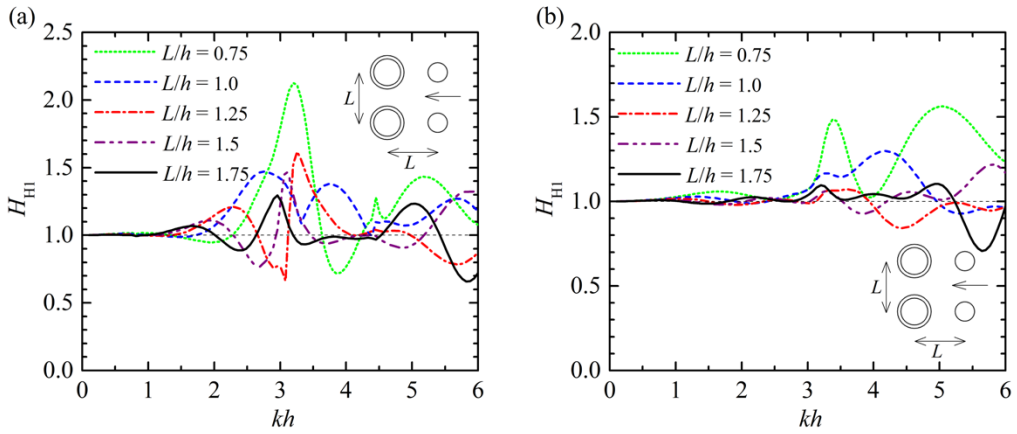


Fig. 15. *H-factor* of the hybrid wave farm ＃H1 versus *kh* for different *L*/*h*, β=π: (a) Case I; (b) Case II.

Figure 16 presents the power capture response of #P1 and #P2 with different *L*/*h* and β=0.25π. Different from those η_{P1} (Case I)-*kh* curves for #P1 with *L*/*h* =0.75, 1.0, 1.25 and 1.75, which have two peaks at least, the one for #P1 with *L*/*h* =1.5 has only one single peak (Fig. 16a). For the #P1 (Case II), Fig. 16b, the η_{P1} (Case II)-*kh* curves have one single peak for *L*/*h* =0.75, 1.0, and 1.75; whereas for *L*/*h*=1.25 and 1.5, there is a second peak, at *kh*=4.9 and 3.9, respectively, where η_{P2} (#P2, Fig. 16c) are also peaked. The improvement for such wave conditions is caused by the diffracted and radiated waves between the WECs in the farm. The larger the *L*/*h*, the smaller the *kh* value for which the improvement induced by the array effect occurs. The single peak of η_{P1} for *L*/*h* =1.75 occurs at *kh*=3.4 (Fig. 16b), which is obviously larger than the *kh* where the peak happens for the farm with different *L*/*h* ratios. Given that η_{P2} peaks at *kh*=3.45 (Fig. 16c), this phase difference may well be caused by hydrodynamic interaction among the WECs.

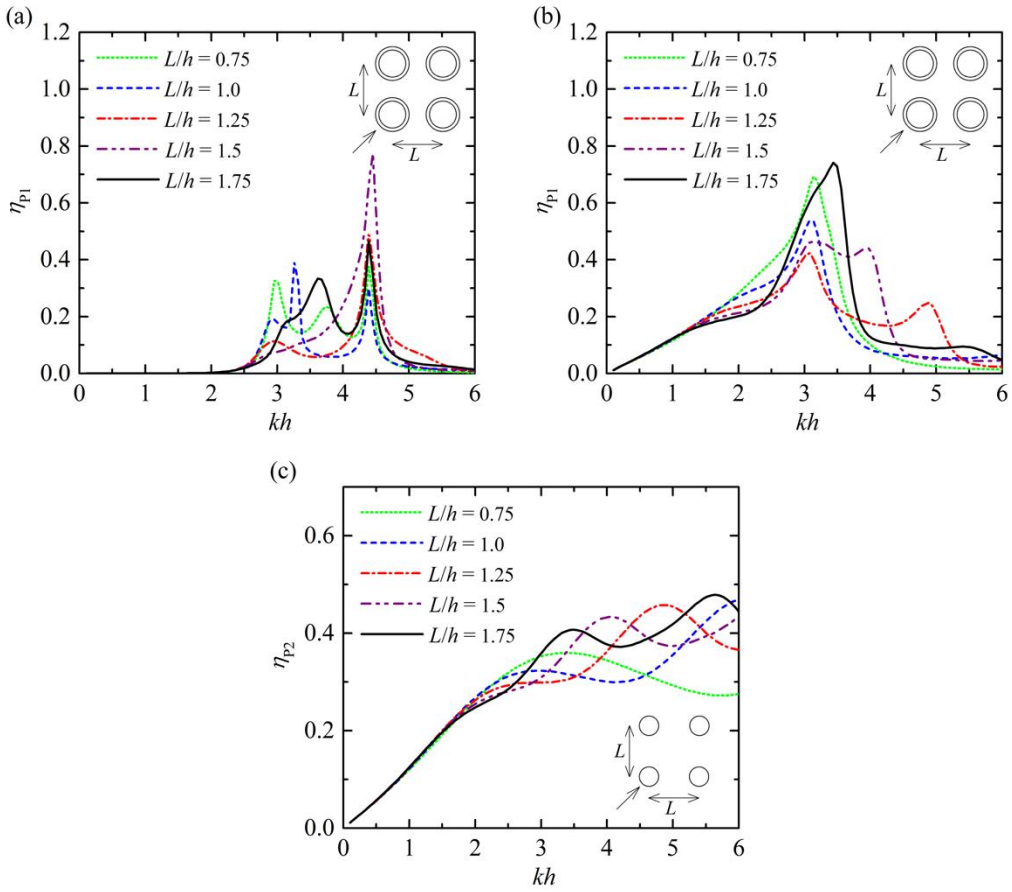


Fig. 16. Power capture factor of the conventional wave farm versus *kh* for different *L*/*h*, $\beta=\pi/4$: (a) OWCs farm of Case I; (b) OWCs farm of Case II; (c) PAs farm.

Figures 17 and 18 present the frequency responses of the power capture factor and *H-factor* of hybrid wave farm #H2 (Cases I and II) for different *L*/*h* values under waves with $\beta=0.25\pi$. The hybrid wave farm #H2 (Case I) with *L*/*h* =0.75 performs much better than the others at *kh*=3.3; nevertheless, it is the worst performer for $4.8<kh<6.0$. This also applies to #H2 (Case II) (Fig. 17b), which is the worst choice even for a larger range of wave conditions. For #H2, Case II (Figs. 17b, 18b), the peaks of η_{H2} and H_{H2} occur at different *kh* for farms with different *L*/*h*. Therefore, changing the ratio *L*/*h* can be used to adjust the hybrid wave farm to specified working wave conditions.

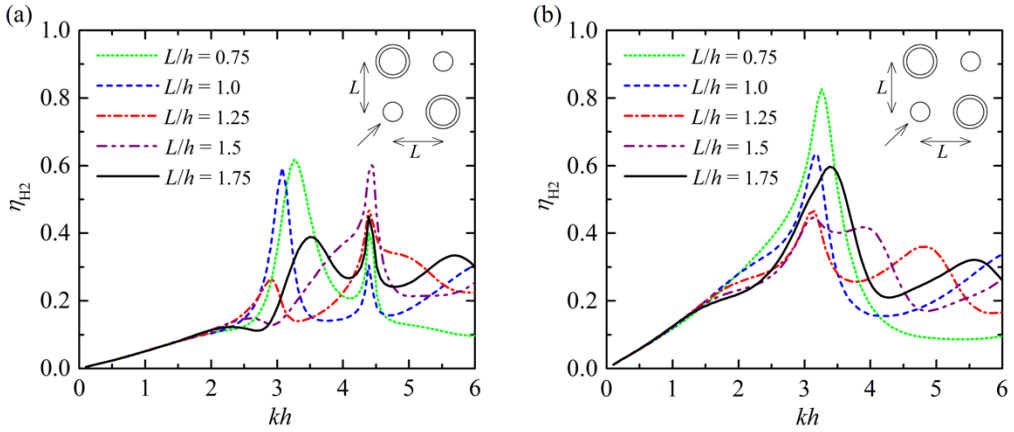


Fig. 17. Power capture factor of the hybrid wave farm #H2 versus kh for different L/h, β= $\pi/4$: (a) Case I; (b) Case II.

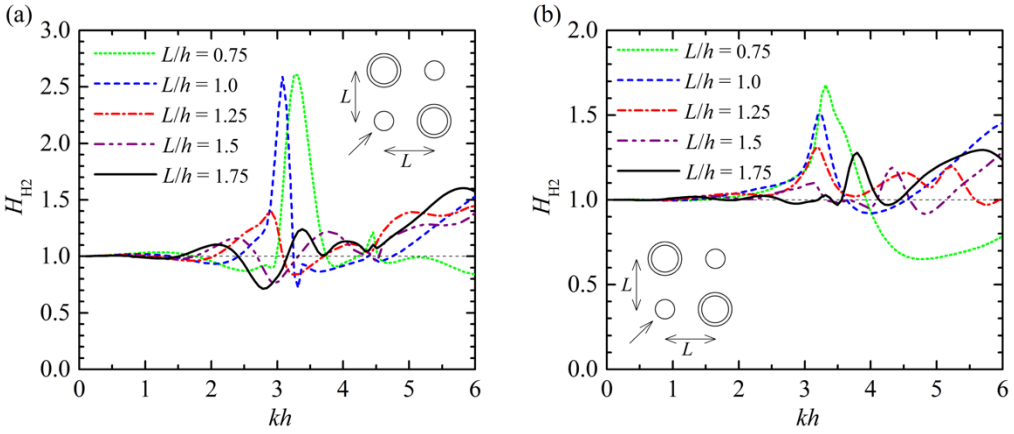


Fig. 18. *H-factor* of the hybrid wave farm #H2 versus kh for different L/h, β= $\pi/4$: (a) Case I; (b) Case II.

3.4 Discussion

In practice, hybrid wave farms may be advantageous relative to conventional (single-device) wave farms in many situations, as proven in the case study. However, it is important to clarify that the theoretical maximum absorbed power over all incidence angles cannot be improved by the hybrid concept. If we consider a hybrid wave farm consisting of M PAs and N fixed OWCs as an example, the expression of the theoretical maximum absorbed power, P_{MAX}, over all incidence angles is

$$\int_0^{2\pi} P_{\mathrm{MAX}}(\beta)\,\mathrm{d}\beta = \frac{(M+N)\pi\rho g v_g A^2}{2k}, \tag{21}$$

the derivation of which is given in Appendix A.

This theoretical maximum absorbed power corresponds to an ideal situation in which the configuration of the wave farm has been optimized and each WEC is controlled optimally, i.e., both damping and stiffness/mass are adopted and ideally optimized. In that case, resonance is achieved by all the WECs in the wave farm. In practice, however, it will often be impossible to attain such an ideal situation. Involving both damping and stiffness/mass in the PTO system

and optimizing them simultaneously may well prove too complicated and expensive in the real world. For this reason, most researchers so far have studied the performance of a wave farm assuming that the PTO system of its WECs consists of PTO damping only (Babarit, 2010; Penalba et al., 2017). Therefore, in the present study of the hybrid effect, and of its quantification by means of an ad hoc *H-factor*, the effect of the PTO system for each WEC is merely represented by a damping coefficient (the effect of air compressibility is also considered as a kind of "added mass" for the OWCs) and the theoretical maximum absorbed power is not considered.

In other words, in the ideal conditions of optimum damping and stiffness/mass for all the WECs, a hybrid wave farm cannot theoretically absorb more energy than a conventional wave farm over all incidence angles. The interest of such conditions is limited, however, given that they are all but impossible to attain in practice. Importantly, in the practical, more easily achievable conditions (i.e., with optimal PTO damping coefficient adopted), a hybrid wave farm can indeed enhance power absorption in certain cases. For example, when the layout of a wave farm is fixed, e.g., due to marine space considerations, or environmental or economic constraints, a conventional wave farm may not be the most efficient option as a result of a destructive array effect; in that case, a hybrid farm may well be more efficient if a constructive hybrid effect occurs. The hybrid effect, which can be quantified through the *H-factor* proposed in this work, may in fact overcome the destructive array effect, as was proven in the case study.

4. Conclusions

In this paper the power performance and the motion and pressure response of a hybrid wave farm were investigated by means of an *ad hoc* semi-analytical model. A novel parameter, the *H-factor*, was proposed to estimate the effect of the hybrid nature of the farm, i.e., of combining different types of WECs, on its power capture performance. More specifically, two configurations consisting of two OWCs and two PAs were considered: parallel (#H1) and diagonal (#H2). The roles of the incident wave direction and the spacing between the WECs were investigated and discussed. The following conclusions may be drawn.

First, the combination of different types of WECs in a hybrid farm may enhance or reduce power capture performance relative to a conventional (single-type) wave farm. This hybrid effect may be easily quantified through the *H-factor*, with $H>1$ or $H<1$ signifying enhanced or reduced performance, i.e., constructive or destructive hybrid effect, respectively. For some specified cases, constructive hybrid effect (i.e., $H>1$) is valid for the whole range of wave conditions studied ($0.1<kh<6.0$), demonstrating the advantages of hybrid wave farms relative to conventional wave farms in certain conditions..

Second, the power capture performance of the farm depends on the type of OWC adopted (free-floating or fixed), the wave conditions (frequency and direction) and the configuration of the farm (#H1 or #H2). For the hybrid wave farm with spacing distance $L/h=0.75$ working in the specified wave conditions, $kh=3.3$, #H1 is found to be a better choice in capturing power from waves with a broad range of incident directions. By contrast, for waves with a narrow range of incident directions, #H2 could be more beneficial to power absorption thanks in part to a constructive hybrid effect, as demonstrated by the *H-factor* taking on a value above unity.

Third, regarding the type of OWC, the hybrid wave farm generally absorbs more power

with the OWCs fixed rather than free floating.

Finally, with respect to the wave frequency, the peak value of the wave capture factor and the corresponding *kh* depend on the *L*/*h* ratio. A second peak of the wave capture factor may be induced by the array effect. In this case, the larger the *L*/*h* ratio, the smaller the frequency *kh* of this second peak.

Acknowledgements

This research was supported by the European Commission, project Intelligent Community Energy (ICE), INTERREG V FCE (Contract No. 5025), the China Postdoctoral Science Foundation (Grant No. 2016M601041, 2017T100085) and the National Natural Science Foundation of China (51679124, 51879144).

Appendix A Theoretical maximum absorbed power over all incidence angles

For an array of independently oscillating PAs capturing wave energy through heave modes only, P_{MAX} satisfies the following identity, integrating over all incidence angles (Wolgamot et al., 2012),

$$\int_0^{2\pi} P_{\mathrm{MAX}}(\beta)\,\mathrm{d}\beta = \frac{N\pi\rho g v_g A^2}{2k}, \tag{A 1}$$

where N represents the number of PAs included in the wave farm. It can be easily proved that Eq. (A 1) is valid as well for an array of fixed OWCs consisting of N devices. Hereinafter, we consider a hybrid wave farm consisting of N WECs, which include both PAs capturing wave energy through heave modes only and fixed OWCs.

The total hydrodynamic force on PAs ($\boldsymbol{F}_{\mathrm{t}}$) and the total volume flow on OWCs ($\boldsymbol{Q}_{\mathrm{t}}$) can be expressed in matrix notation as (Falnes, 2002)

$$\begin{bmatrix}\boldsymbol{F}_{\mathrm{t}}\\ \boldsymbol{Q}_{\mathrm{t}}\end{bmatrix} = \begin{bmatrix}\boldsymbol{F}\\ \boldsymbol{Q}\end{bmatrix} - \begin{bmatrix}\mathbf{Z} & \mathbf{H}\\ -\mathbf{H}^{\mathrm{T}} & \mathbf{Y}\end{bmatrix}\begin{bmatrix}\boldsymbol{u}\\ \boldsymbol{p}\end{bmatrix}, \tag{A 2}$$

where the first term represents the excitation quantities and the last term the radiation problem. $\boldsymbol{u}$ and $\boldsymbol{p}$ denote the velocity vector of PAs and the air pressure of OWCs, respectively. $\mathbf{Z}$, $\mathbf{H}$ and $\mathbf{Y}$ are radiation matrices, which can be decomposed into their real and imaginary parts:

$$\mathbf{Z} = \mathbf{R} - \mathrm{i}\mathbf{X}, \tag{A 3a}$$

$$\mathbf{Y} = \mathbf{G} - \mathrm{i}\mathbf{B}, \tag{A 3b}$$

$$\mathbf{H} = \mathbf{C} - \mathrm{i}\mathbf{J}. \tag{A 3c}$$

Following Evans (1980), Falnes (1980) and Falnes (2002), the theoretical maximum power that may be extracted by the hybrid wave farm can be expressed as

$$P_{\mathrm{MAX}}(\beta) = \frac{1}{8}\mathbf{Q}_{\mathrm{e}}^{\dagger}(\beta)\mathbf{S}^{-1}\mathbf{Q}_{\mathrm{e}}(\beta), \tag{A 4}$$

where

$$\boldsymbol{Q}_{\mathrm{e}}=\begin{bmatrix}\boldsymbol{F}\\ -\boldsymbol{Q}\end{bmatrix},\ \text{and}\ \ \mathbf{S}=\begin{bmatrix}\mathbf{R} & \mathrm{i}\mathbf{J}\\ -\mathrm{i}\mathbf{J}^{\mathrm{T}} & \mathbf{G}\end{bmatrix}. \tag{A 5}$$

The theoretical maximum absorbed power as shown in Eq. (A 4) is obtained when an ideal PTO system is applied, such that

$$\begin{bmatrix}\boldsymbol{u}\\ -\boldsymbol{p}\end{bmatrix}=\frac{1}{2}\mathbf{S}^{-1}\boldsymbol{Q}_{\mathrm{e}}. \tag{A 6}$$

Note **S** is a complex Hermitian matrix, which can be written as the product of an upper real triangular matrix **H** and its transpose with the employment of the Cholesky decomposition,

$$\mathbf{S}=\mathbf{H}^{\mathrm{T}}\mathbf{H}, \tag{A 7}$$

hence,

$$\mathbf{S}^{-1}=\mathbf{H}^{-1}\left(\mathbf{H}^{\mathrm{T}}\right)^{-1}. \tag{A 8}$$

For the sake of convenience, a column vector is defined as

$$\boldsymbol{W}\left(\beta\right)=\left(\mathbf{H}^{\mathrm{T}}\right)^{-1}\boldsymbol{Q}_{\mathrm{e}}\left(\beta\right), \tag{A 9}$$

from which Eq. (A 4) can be rewritten as

$$P_{\mathrm{MAX}}\left(\beta\right)=\frac{1}{8}\boldsymbol{W}^{\dagger}\left(\beta\right)\boldsymbol{W}\left(\beta\right). \tag{A 10}$$

Using the Haskind relation, **S** can be rewritten with the integral of $\boldsymbol{Q}_{\mathrm{e}}$ over all incidence angles as (Zheng and Zhang, 2018)

$$\mathbf{S}=\frac{k}{8\pi\rho g v_{\mathrm{g}}A^{2}}\int_{0}^{2\pi}\boldsymbol{Q}_{\mathrm{e}}\left(\beta\right)\boldsymbol{Q}_{\mathrm{e}}^{\dagger}\left(\beta\right)\mathrm{d}\beta. \tag{A 11}$$

Multiplying two **H** related inverse matrices results in

$$\left(\mathbf{H}^{\mathrm{T}}\right)^{-1}\mathbf{S}\mathbf{H}^{-1}=\frac{k}{8\pi\rho g v_{\mathrm{g}}A^{2}}\int_{0}^{2\pi}\boldsymbol{W}\left(\beta\right)\boldsymbol{W}^{\dagger}\left(\beta\right)\mathrm{d}\beta=\mathbf{I}, \tag{A 12}$$

leading to the integral

$$\int_{0}^{2\pi}W_{i}\left(\beta\right)W_{j}^{*}\left(\beta\right)\mathrm{d}\beta=\delta_{i,j}\frac{8\pi\rho g v_{\mathrm{g}}A^{2}}{k}. \tag{A 13}$$

Integrating Eq. (A 10) over $\beta \in [0,2\pi]$ and adopting Eq. (A 13) gives

$$\int_0^{2\pi} P_{\mathrm{MAX}}(\beta)\,\mathrm{d}\beta = \frac{N\pi\rho g v_{\mathrm{g}} A^2}{k}, \qquad \text{(A 14)}$$

implying that the expression of the theoretical maximum absorbed power over all incidence angles as given in Eq. (A 1) holds as well for a hybrid wave farm (see Eq. (A 14)). In other words, the theoretical maximum absorbed power over all incidence angles cannot be improved by the hybrid concept.

References

Andrés, A.D., Guanche, R., Meneses, L., et al., 2014. Factors that influence array layout on wave energy farms. Ocean Engineering. 82, 32-41.

Astariz, S, Iglesias, G, 2016a. Selecting optimum locations for co-located wave and wind energy farms. PART I: the Co-Location Feasibility index. Energy Conversion and Management, 122, 589-598.

Astariz, S, Iglesias, G, 2016b. Selecting optimum locations for co-located wave and wind energy farms. PART II: a case study. Energy Conversion and Management, 122, 599-608.

Astariz, S., Iglesias, G, 2016c. Wave energy vs. other energy sources: a reassessment of the economics. International Journal of Green Energy 2016, 13, 744-755. Taylor & Francis.

Astariz, S, Iglesias, G, 2016d. Co-located wind and wave energy farms: Uniformly distributed arrays. Energy 113, pp. 497-508,

Astariz, S, Iglesias, G, 2016e. Hybrid wave and offshore wind farms: a comparative case study of co-located layouts. International Journal of Marine Energy, 15, pp. 2-16,

Astariz, S, Iglesias, G, 2016f. Output power smoothing and reduced downtime period by combined wind and wave energy farms, Energy, 97, 69-81.

Astariz, S, Iglesias, G, 2017. The Collocation Feasibility Index - a method for selecting sites for co-located wave and wind farms. Renewable Energy, 103, pp. 811-824.

Astariz, S, Vazquez, A, Sanchez, M, Carballo, R, Iglesias, G, 2018. Co-located wave-wind farms for improved O&M efficiency. Ocean and Coastal Management, 163, pp. 66-71.

Babarit, A., 2010. Impact of long separating distances on the energy production of two interacting wave energy converters. Ocean Engineering. 37, 718-729.

Babarit, A., 2013. On the park effect in arrays of oscillating wave energy converters. Renewable Energy. 58, 68-78.

Borgarino, B., Babarit, A., Ferrant, P., 2012. Impact of wave interactions effects on energy absorption in large arrays of wave energy converters. Ocean Engineering. 41, 79-88.

Carballo, R., Iglesias, G., 2012. A methodology to determine the power performance of wave energy converters at a particular coastal location, Energy Conversion and Management, 61, pp. 8-18.

Carballo, R, Sanchez, M, Ramos, JV, Fraguela, JA, Iglesias, G, 2015a. The intra-annual variability in the performance of wave energy converters: a comparative study in N Galicia (Spain), Energy, 82, pp. 138-146.

Carballo, R, Sanchez, M, Ramos, V, Fraguela, JA, Iglesias, G, 2015b. Intra-annual wave

resource characterization for energy exploitation: a new decision-aid tool, Energy Conversion and Management, 93, pp. 1-8.

Carballo, R, Arean, N, Alvarez, M, Castro, A, Lopez, M, Iglesias, G, 2019. Wave farm planning through high-resolution resource and performance characterization, Renewable Energy, 135, pp. 1097-1107.

Contestabile, P., Di Lauro, E., Buccino, M., Vicinanza, D., 2016. Economic assessment of Overtopping BReakwater for Energy Conversion (OBREC): a case study in Western Australia, Sustainability, 9, 51.

Elhanafi, A., Macfarlane, G., Ning, D., 2018. Hydrodynamic performance of single-chamber and dual-chamber offshore-stationary Oscillating Water Column devices using CFD. Applied Energy, 228, 82-96.

Evans, D.V., 1980. Some analytic results for two- and three-dimensional wave-energy absorbers. In: Count, B. (Ed.), Power from Sea Waves. Academic Press, 213-249.

Falnes, J., 1980. Radiation impedance matrix and optimum power absorption for interacting oscillators in surface waves. Applied Ocean Research. 2, 75-80.

Falnes, J., 2002. Ocean waves and oscillating systems. Cambridge University Press, Cambridge, UK.

Fitzgerald, C., Thomas, G., 2007. A preliminary study on the optimal formation of an array of wave power devices. Proceedings of the 7th European Wave and Tidal Energy Conference.

Göteman, M., 2017. Wave energy parks with point-absorbers of different dimensions. Journal of Fluids and Structures. 74, 142-157.

Guo, B., Patton, R. J., Jin, S., Lan, J., 2018. Numerical and experimental studies of excitation force approximation for wave energy conversion. Renewable Energy. 125, 877-889.

He, F., Zhang, H., Zhao, J., Zheng, S., Iglesias, G., 2019. Hydrodynamic performance of a pile-supported OWC breakwater: An analytical study. Applied Ocean Research.88, 326-340.

Konispoliatis, D.N., Mavrakos, S.A., 2016. Hydrodynamic analysis of an array of interacting free-floating oscillating water column (OWC's) devices. Ocean Engineering. 111, 179-197.

Lopez, I., Pereiras, B., Castro, F., Iglesias, G., 2014. Optimisation of turbine-induced damping for an OWC wave energy converter using a RANS-VOF numerical model. Applied Energy. 127, 105-114.

Lopez, I, Pereiras, B, Castro, F, Iglesias, G, 2016. Holistic performance analysis and turbine-induced damping for an OWC wave energy converter. Renewable Energy, 85, pp. 1155-1163.

Lovas, S., Mei, C.C., Liu, Y., 2010. Oscillating water column at a coastal corner for wave power extraction. Applied Ocean Research. 32(3), 267-283.

Martins-rivas, H., Mei, C.C., 2009. Wave power extraction from an oscillating water column along a straight coast. Ocean Engineering, 36(6-7), 426-433.

Malara, G, Arena, F, 2013. Analytical modelling of an U-Oscillating Water Column and performance in random waves. Renewable Energy, 60, 116-126.

Mavrakos, S.A., Kalofonos, A., 1997. Power absorption by arrays of interacting vertical axisymmetric wave-energy devices. Journal of Offshore Mechanics and Arctic Engineering. 119(4), 244-251.

McIver, P., Mavrakos, S.A., Singh, G., 1995. Wave-power absorption by arrays of devices.

Proceedings of the 2nd European Wave Power Conference, Lisbon, Portugal, 126-133.
Nader, J.R., 2013. Interaction of ocean waves with oscillating water column wave energy convertors. University of Wollongong, Australia, PhD.
Penalba, M., Touzón, I., Lopez-Mendia,J., et al., 2017. A numerical study on the hydrodynamic impact of device slenderness and array size in wave energy farms in realistic wave climates. Ocean Engineering. 142, 224-232.
Perez-Collazo, C, Greaves, D, Iglesias, G, 2018a. A Novel Hybrid Wind-Wave Energy Converter for Jacket-Frame Substructures. Energies. 11 (3), 637.
Perez-Collazo, C, Greaves, D, Iglesias, G, 2018b. Hydrodynamic response of the WEC sub-system of a novel hybrid wind-wave energy converter. Energy Conversion and Management. 171, 307-325.
Renzi, E., Abdolali, A., Bellotti, G., et al., 2014. Wave-power absorption from a finite array of oscillating wave surge converters. Renewable Energy. 63, 55-68.
Ricci, P., Saulnier, J.B., Falcas, A., 2007. Point-absorbers arrays: a configuration study off the portuguese west-coast. Proceedings of the 7th European Wave and Tidal Energy Conference, Porto, Portugal, September 11-13.
Sarkar, D., Renzi, E., Dias, F., 2014. Wave farm modelling of oscillating wave surge converters. Proceedings of the Royal Society A. 470: 20140118.
Veigas, M, Iglesias, G, 2014. Potentials of a hybrid offshore farm for the island of Fuerteventura, Energy Conversion and Management, 86, pp. 300-308.
Veigas, M., López, M., Iglesias, G., 2014. Assessing the optimal location for a shoreline wave energy converter. Applied Energy. 132, 404-411.
Veigas, M., López, M., Romillo, P., Carballo, R., Castro, A., Iglesias, G., 2015. A proposed wave farm on the Galician coast. Energy Conversion and Management. 99, 102-111.
Wolgamot, H.A., Taylor, P.H., Eatock Taylor, R., 2012. The interaction factor and directionality in wave energy arrays. Ocean Engineering. 47, 65-73.
Wu, J., Shekh, S., Sergiienko, N.Y., et al., 2016. Fast and effective optimisation of arrays of submerged wave energy converters. Proceedings on Genetic and Evolutionary Computation Conference. July 20 – 24, Denver, Colorado, USA. 1045-1052.
Zheng, S., Zhang, Y., 2018. Theoretical modelling of a new hybrid wave energy converter in regular waves. Renewable Energy. 128, 125-141.
Zheng, S., Zhang, Y., Iglesias, G., 2018. Wave-structure interaction in hybrid wave farms. Journal of Fluids and Structures. 83, 386-412.
Zheng, S., Antonini, A., Zhang, Y., Greaves, D., Miles, J., Iglesias, G., 2019a. Wave power extraction from multiple oscillating water columns along a straight coast. Journal of Fluid Mechanics. 878, 445-480.
Zheng, S., Zhang, Y., Iglesias, G., 2019b. Coast/breakwater-integrated OWC: A theoretical model. Marine Structures. 66, 121-135.
Zhong, Q., Yeung, R.W., 2019. Wave-body interactions among energy absorbers in a wave farm. Applied Energy. 233-234, 1051-1064.